JOURNAL OF PETROLOGY | VOLUME 0 | NUMBER 0 | PAGES 1–30 | 2012 | doi:10.1093/petrology/egs078
Journal of Petrology Advance Access published December 4, 2012

Magmatic Recharge during the Formation and Resurgence of the Valles Caldera, New Mexico, USA: Evidence from Quartz Compositional Zoning and Geothermometry

JACK WILCOCK[1], FRASER GOFF[2], WILLIAM G. MINARIK[1] AND JOHN STIX[1]*

[1]DEPARTMENT OF EARTH AND PLANETARY SCIENCES, MCGILL UNIVERSITY, MONTRÉAL, QUÉBEC H3A 2A7, CANADA
[2]DEPARTMENT OF EARTH AND PLANETARY SCIENCES, UNIVERSITY OF NEW MEXICO, ALBUQUERQUE, NM 87131, USA

RECEIVED JANUARY 3, 2011; ACCEPTED OCTOBER 4, 2012

The Valles Caldera complex in north–central New Mexico, USA, represents the type example of a resurgent caldera system, characterized by eruption of two voluminous high-silica rhyolite ignimbrites, the Otowi and Tshirege Members of the Bandelier Tuff. Central resurgence of ~1000 m occurred within 27 ± 27 kyr following eruption of the Tshirege, or Upper Bandelier Tuff (UBT). This process was accompanied by small-volume eruptions of the Deer Canyon Rhyolite, followed closely by the Redondo Creek Rhyodacite. The Cerro del Medio Rhyolite lava dome complex is a product of ring fracture volcanism following resurgence. We have combined cathodoluminescence (CL) imaging and titanium-in-quartz geothermometry techniques for single quartz crystals from (1) different stratigraphic horizons of the UBT ignimbrite, (2) samples of the Deer Canyon Rhyolite and (3) the Cerro del Medio Rhyolite lavas to build an evolutionary model of the Valles Caldera lifecycle. CL imaging reveals that ~70% by volume of the UBT ignimbrite contains unzoned quartz crystals (average concentration 28 ± 2 ppm Ti), recording relatively stable conditions. The abrupt appearance of compositionally zoned quartz crystals within the mid-to-late erupted UBT ignimbrite units 3–5 reveals evidence for interaction with hotter magma. Corresponding titanium-in-quartz measurements of outer, high-intensity CL rims (average of 71 ± 9 ppm Ti) reveal temperature increases of between ~35 and 140°C relative to the initial, volumetrically large Upper Member eruptions (flow units 1 and 2). These temperature increases mimic those originally reported in the literature. Compared with the temperature increases, changes in pressure appear to play a secondary role. We have also discovered an interesting heterogeneity within the Deer Canyon Rhyolite lavas, with strong spatial control on the eruption of porphyritic lavas containing complexly zoned quartz crystals on the western parts of the resurgent dome. Conversely, crystal-poor to aphyric lavas containing small, unzoned quartz crystals are confined to eastern parts of the resurgent dome. The Cerro del Medio Rhyolite lavas are sparsely porphyritic to aphyric, and contain unzoned quartz with titanium concentrations more than 40 ppm higher than the cores of UBT quartz. The quartz-free Redondo Creek Rhyodacite is the most primitive silicic material erupted during the Valles Caldera cycle. Intrusion of this hotter magma into a residual UBT crystal mush zone may have facilitated eruption and geochemical–thermal heterogeneity within the Deer Canyon Rhyolite, resurgence of the caldera, and expulsion of hot, crystal-poor rhyolite batches from the mush zone, which were subsequently erupted as the Cerro del Medio complex.

KEY WORDS: *calderas; cathodoluminescence; geothermometry; ignimbrites; Valles Caldera; Bandelier Tuff*

INTRODUCTION

Magmatic recharge is an important issue in volcanology, not least because this process thermally sustains long-lived magmatic systems and also serves as a potential eruption trigger. Recharge events have been recorded at many large silicic centres (e.g. Taupo, New Zealand; Long

*Corresponding author. Phone: +1 514 398 5391. Fax: +1 514 398 4680. E-mail: stix@eps.mcgill.ca

Valley, California, USA; Valles, New Mexico, USA; Yellowstone, Wyoming, USA), which have undergone multiple eruptive episodes over time intervals of the order of several million years (e.g. Wark *et al.*, 2007; Shane *et al.*, 2008; Campbell *et al.*, 2009; Girard & Stix, 2009; Vasquez *et al.*, 2009; Smith *et al.*, 2010). The evolution of large silicic centres is linked to the duration and rate of magmatic recharge, which in turn controls the repose time and volume of successive eruptive events (Smith, 1979; Spera & Crisp, 1981; Lipman, 2007; Annen, 2009). Magmatic systems of this size often produce caldera-forming eruptions. After caldera formation, some structures undergo resurgence, whereby the caldera floor is substantially uplifted. Several studies suggest that resurgence is largely driven by magmatic recharge in response to the partial draining of the magma chamber during an eruption (Smith & Bailey, 1966; Lipman, 1984; Cole *et al.*, 2005; Acocella, 2010). The Valles Caldera located in the Jemez Mountains Volcanic Field, north–central New Mexico, USA, represents the type example of a resurgent caldera as identified in the seminal work of Smith & Bailey (1966, 1968) (Fig. 1a and b). Silicic volcanism has spanned roughly 2 Myr, punctuated by the eruption of two voluminous, high-silica rhyolite ignimbrites (the Otowi and Tshirege Members of the Bandelier Tuff) totalling 800 km^3 dense rock equivalent (DRE) of pyroclastic material (Fig. 1b; Smith & Bailey, 1966; Smith, 1979; Heiken *et al.*, 1990; Goff, 2010). Petrological textures of the youngest lavas in the caldera (Wolff & Gardner, 1995) and tomographic imaging studies (Steck *et al.*, 1998; Aprea *et al.*, 2002) suggest that silicic melt is being generated by remelting of an underlying relict crystal mush zone by injection of new magma. This evidence implies that the Valles Caldera could potentially erupt again in the future (Wolff & Gardner, 1995; Steck *et al.*, 1998). Therefore, the Valles Caldera remains a site of continued interest in understanding the role of magmatic recharge in the caldera lifecycle.

Recent $^{40}Ar/^{39}Ar$ geochronology work has shown that central resurgence of ~1000 m occurred rapidly within 54 kyr of the eruption of the Tshirege or Upper Bandelier Tuff (UBT) (Phillips *et al.*, 2007*b*). Thus, recharge was almost certainly occurring immediately following eruption of the UBT, and was a major control upon resurgence.

In this study, we report the results of cathodoluminescence (CL) imaging and *TitaniQ* titanium-in-quartz geothermometry (Wark & Watson, 2006; Thomas *et al.*, 2010; Huang & Audétat, 2012) on single quartz crystals sampled from (1) all ignimbrite flow units of the UBT, (2) lavas erupted during resurgence (Deer Canyon Rhyolite and Redondo Creek Rhyodacite) and (3) the first lavas erupted into the caldera ring fracture zone immediately following resurgence (Cerro del Medio Rhyolite). We have generated an evolutionary model of the Bandelier magmatic system from ~1·25 to ~1·1 Ma, establishing relative magmatic temperatures during (1) pre-eruption periods, (2) the cataclysmic UBT eruption, (3) resurgence and (4) initial ring fracture volcanism.

In this study we call attention to the Redondo Creek Rhyodacite (Goff *et al.*, 2011), which was erupted immediately after the Deer Canyon Rhyolite during resurgence and represents the most primitive silicic material erupted during the Valles Caldera cycle. The lack of quartz within this unit precludes analysis by *TitaniQ*, yet the occurrence of the Redondo Creek Rhyodacite is significant for magma chamber processes following a caldera-forming eruption. Other large silicic calderas have erupted rhyodacite lavas contemporaneously with resurgence; for example, Long Valley (Hildreth, 2004), Okataina, New Zealand (Shane *et al.*, 2005), Taupo, New Zealand (Smith *et al.*, 2005) and Yellowstone (Girard & Stix, 2009). It is possible that this material may represent the product of magmatic recharge into a residual crystal mush following caldera collapse. Results from this study further highlight the important role of magmatic recharge in the caldera lifecycle.

Geological setting and caldera-forming eruptions in the Jemez Mountains

The Jemez Mountains Volcanic Field (JMVF) in north–central New Mexico comprises a Miocene–Quaternary suite of basaltic to rhyolitic rocks that are an expression of volcanism occurring at the intersection of the north–south-trending Rio Grande Rift (RGR) and the NE–SW-trending Jemez Lineament (Fig. 1b; Aldrich *et al.*, 1986; Self *et al.*, 1986; Heiken *et al.*, 1990; Wolff *et al.*, 2002; Goff & Gardner, 2004; Phillips *et al.*, 2007*b*; Rowe *et al.*, 2007). Palaeostress determinations show that regional east–west extension of the RGR commenced around 32 Ma and continues episodically to the present (Aldrich *et al.*, 1986). A tectonic lull from 18 to 13 Ma preceded renewed extension and formation of much of the JMVF within a several million year period (Rowe *et al.*, 2007). From seminal work conducted by Bailey *et al.* (1969) and later revised by Gardner *et al.* (2010), the formalized stratigraphy divides the rocks of the JMVF into the Keres and Tewa Groups (oldest to youngest, respectively; see Goff *et al.*, 2011).

Of most relevance to this study, the Tewa Group (1·85 ± 0·07 Ma to 40 ± 6 ka) consists of the La Cueva, Otowi and Tshirege Members of the Bandelier Tuff, Cerro Toledo Formation and Valles Rhyolite (Bailey *et al.*, 1969; Gardner *et al.*, 1986, 2010; Heiken *et al.*, 1990; Fig. 1b). For the purpose of this study, we concentrate on the Upper (Tshirege) Member of the Bandelier Tuff and the first-erupted members of the Valles Rhyolite Formation: the Deer Canyon Rhyolite, the Redondo Creek Rhyodacite and the Cerro del Medio Rhyolite (Fig. 1b).

The Tshirege or Upper Member of the Bandelier Tuff (UBT) (Bailey *et al.*, 1969) followed an ~350 kyr hiatus in

large, ignimbrite-forming eruptions. Eruption of this ~400 km^3 (DRE) ignimbrite at 1·256 ± 0·010 Ma (Phillips *et al.*, 2007*b*) initiated collapse of the Valles Caldera, overprinting the earlier Toledo Caldera, which was formed during the eruption of the Otowi Member Bandelier Tuff at 1·609 ± 0·008 Ma (Spell *et al.*, 1996; Goff, 2010). The UBT is composed of two main deposits. The rhyolitic basal pumice fall, named the Tsankawi Pumice Bed (Bailey *et al.*, 1969), consists of four coarse pumice-fall units and two finer-grained fall units. Each unit has various dispersal patterns (Self *et al.*, 1986) with a maximum aggregate thickness of 3·5 m. The Tsankawi Pumice Bed underlies a sequence of non-welded to densely welded rhyolitic pyroclastic flows that are distributed radially

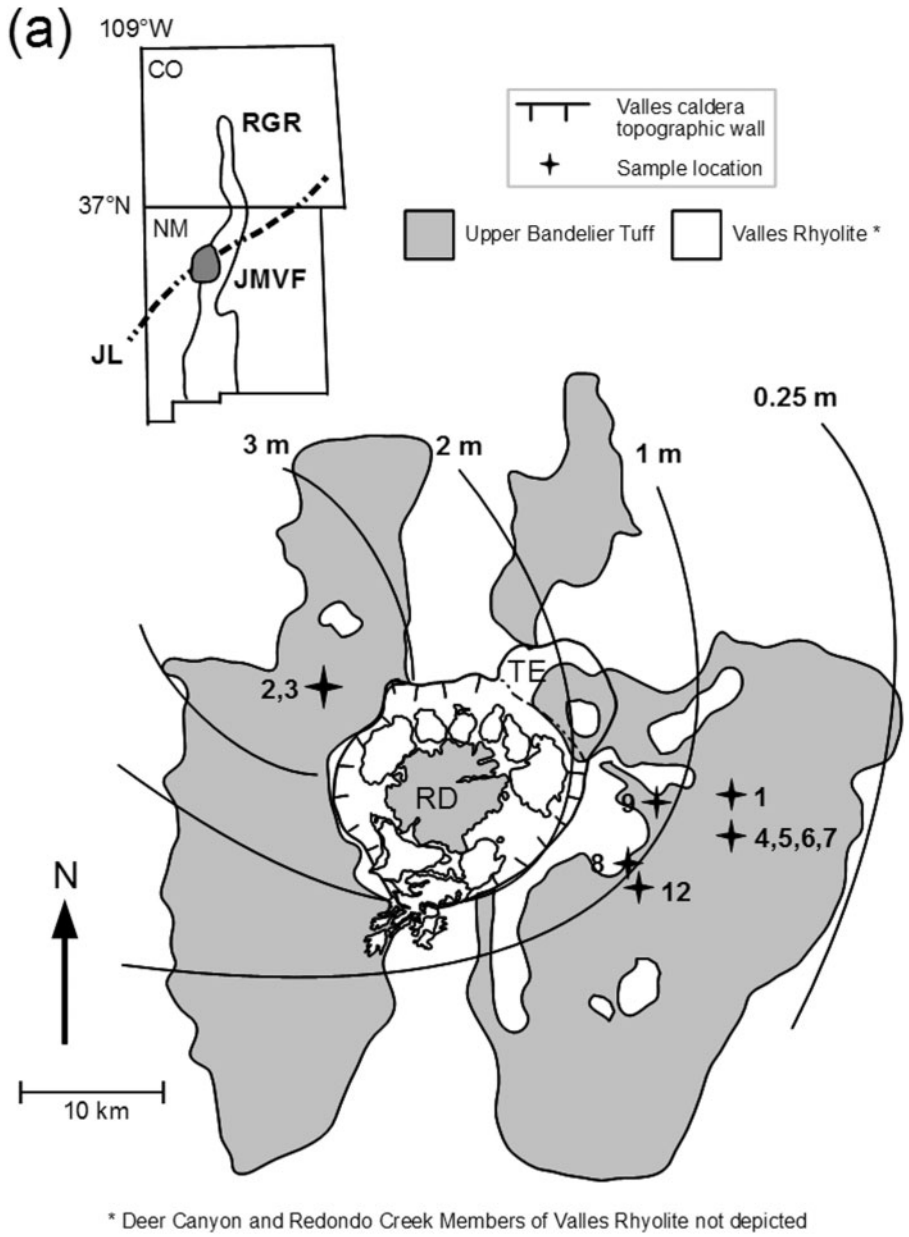

Fig. 1. (a) Regional geological setting of the Jemez Mountains Volcanic Field (JMVF), New Mexico, USA. Map depicts spatial distribution of the Upper Bandelier Tuff (UBT) outflow sheets, spread radially from the Valles Caldera, and the thickness (in metres) of the Tsankawi plinian fallout unit B of Self *et al.* (1986). RGR, Rio Grande rift; JL, Jemez Lineament; RD, resurgent dome; TE, Toledo embayment. (b) Generalized intracaldera geological map of the Valles Caldera and stratigraphy applicable to this study (from Goff *et al.*, 2007, 2011). CdM, Cerro del Medio Rhyolite; RP, Redondo Peak. ^{40}Ar/^{39}Ar ages from Spell *et al.* (1993) and Phillips *et al.* (2007*b*).

(continued)

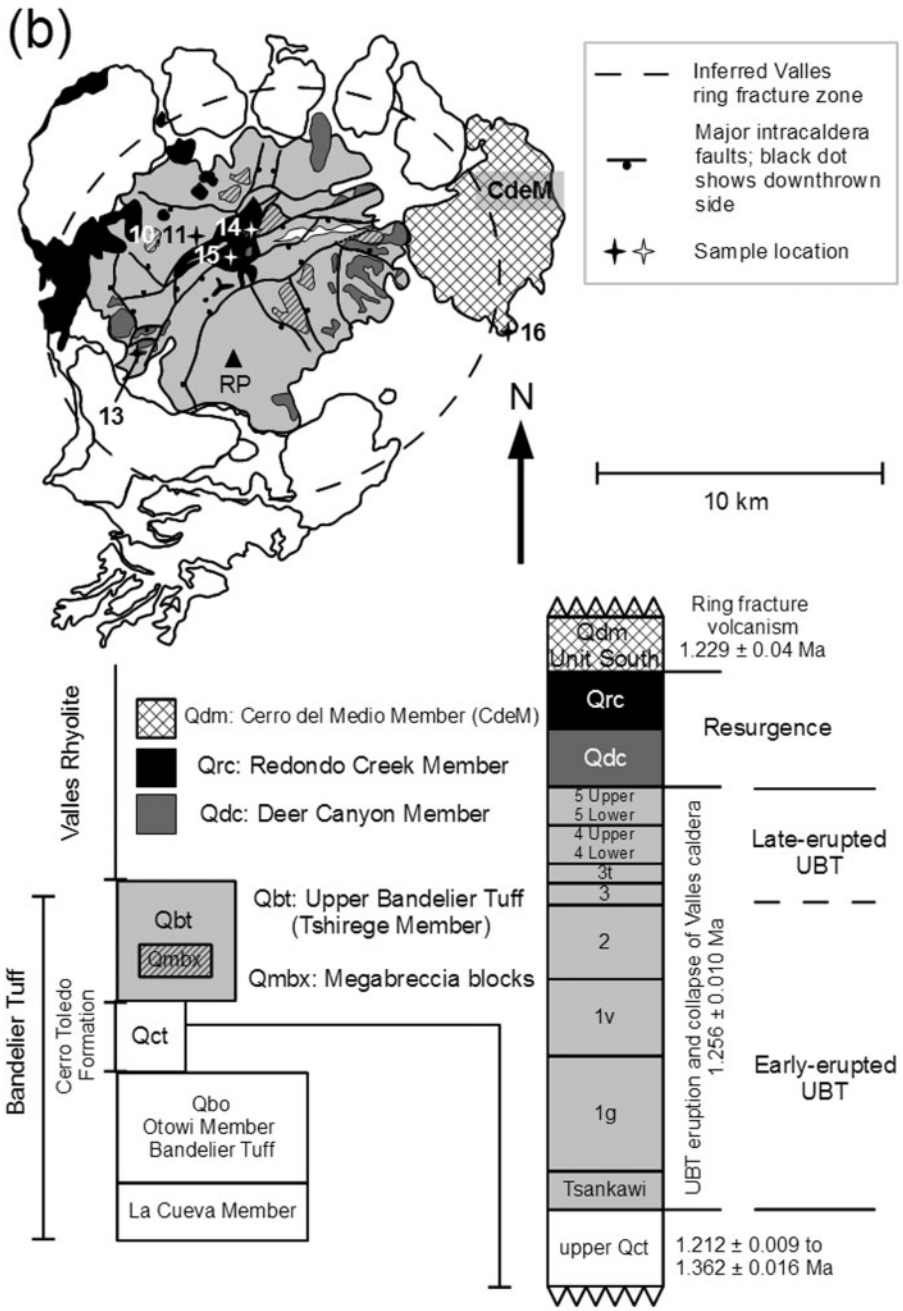

Fig. 1. (Continued).

from the Valles Caldera (Fig. 1a). Extra-caldera thicknesses range from 15 to >270 m and from 400 to >1100 m within the caldera (Nielson & Hulen, 1984; Heiken *et al.*, 1990). In comparison with the Otowi, the UBT is chemically and petrographically stratified, originating from a zoned magma chamber (Smith & Bailey, 1966; see below).

The UBT displays three dominant magmatic components: (1) early erupted high-silica rhyolite (76–78 wt % SiO_2) to late-erupted low-silica rhyolite (~73 wt % SiO_2); (2) distinctive hornblende dacite (69 wt % SiO_2) pumices first appearing within the Tsankawi Pumice Bed and sporadically interspersed within early erupted flow units of the UBT (Bailey *et al.*, 1969; Self & Lipman, 1989; Broxton & Rogers, 2007); (3) syenitic crystal 'clots', which are prominent within late-erupted units (Caress, 1995, 1996; Stimac, 1996). Based on petrological, geochemical and field studies over the last 25 years, the UBT pyroclastic flows are classified as a compound cooling unit constructed of six

principal flow units (1, 2, 3, 3t, 4 and 5; Broxton & Rogers, 2007; Warren *et al.*, 2007). Flow units 1 and 2 represent roughly 70% of the volume of the UBT (roughly 280 km^3).

The Valles Rhyolite (Griggs, 1964; Bailey *et al.*, 1969; Gardner *et al.*, 2010) comprises lava domes, lava flows and pyroclastic units erupted within the Valles Caldera following eruption of the UBT (Fig. 1b). This group covers all units emplaced from 1·256 to 0·04 Ma, and is the result of central caldera resurgence progressing to ring fracture volcanism, although recent studies have highlighted the heterogeneity among successive domes within the caldera (e.g. Spell & Kyle, 1989; Spell *et al.*, 1996). The Deer Canyon Member (1·229–1·283 Ma) includes small-volume high-silica rhyolite lavas, lithic tuffs and breccias emplaced onto the NE and SW flanks of the actively growing resurgent dome immediately after the UBT eruption (Goff & Gardner, 2004; Phillips *et al.*, 2007*a*, 2007*b*; Goff *et al.*, 2011). From stratigraphic relations and refined geochronology, this unit slightly predates the Redondo Creek Member (1·208–1·239 Ma), a series of rhyodacite lavas erupted during the mid-to-late stage of resurgence onto the central and west portions of the dome, and also within the western caldera moat (Phillips *et al.*, 2007*a*, 2007*b*; Goff *et al.*, 2011; Fig. 1b). Both resurgence-related units are interbedded with caldera fill sediments of lacustrine and fluvial origin, which are products of an intracaldera lake environment present before resurgence was initiated (Goff *et al.*, 2007, 2011).

Seven progressively younging high-silica rhyolite dome complexes represent the products of ring fracture volcanism following termination of resurgence within the Valles Caldera. The oldest complex, Cerro del Medio, erupted at 1·229 ± 0·017 Ma (Fig. 1b; Phillips *et al.*, 2007*b*), and comprises five rhyolite lava flows with at least two associated pyroclastic flow deposits; it has a cumulative volume of ~5 km^3 (Gardner *et al.*, 2007).

State of the Bandelier magma chamber during the formation of the Valles Caldera

In their landmark paper, Smith & Bailey (1966) documented vertical 'gradients' in welding, porosity, mineralogy and chemistry of the Upper Bandelier Tuff that provide evidence for sequential eruptions from a thermally stratified, chemically zoned magma chamber (Figs 2 and 3). Initial eruptions were relatively silicic, whereas the final eruptions were more mafic. Based on welding and crystallization experiments, Smith & Bailey (1966) postulated initial emplacement temperatures of 550°C and final emplacement temperatures of over 800°C. Later, Warshaw & Smith (1988) used mineral geothermometers to calculate *in situ* temperatures and oxygen fugacities for the separate magma batches that form the Upper Bandelier ignimbrite sequence. Their results indicate that Tsankawi pumice-fall deposits, representing the silicic top of the magma chamber, equilibrated at about 700°C, whereas the uppermost Tshirege pyroclastic flows, originating from a relatively more mafic zone deeper in the chamber, equilibrated at roughly 850°C (Table 1). Thus, dramatic temperature gradients appear to have existed in the Bandelier magma chamber during the eruption.

The pressure in the pre-eruptive Bandelier magma chamber has been constrained by several means. Sommer (1977) analyzed the volatile contents of silicate melt inclusions in Tshirege quartz phenocrysts and concluded that equilibration occurred at about 150 MPa. This places the top of the chamber at about 5 km depth. More recent work on melt inclusions by Dunbar & Hervig (1992) and Stix & Layne (1996), using secondary ion mass spectrometry (SIMS) techniques, has revealed a range of water contents in the Tsankawi Pumice Bed from 2·7 to 6·2 wt % H_2O, with most samples falling between 4 and 6 wt % H_2O. This range of water translates to minimum pressures of ~85–180 MPa. Warshaw & Smith (1988) determined that coexisting fayalite and orthopyroxene in mid-level Bandelier pyroclastic flows crystallized at pressures between 150 and 200 MPa (5–7 km depth). They stated that 'a pressure somewhat less than 2 kbar (200 MPa) indicates a shallow depth for a significant portion of the Bandelier magma chamber'. Nielson & Hulen (1984) used a structural model to estimate depth to the present top of the crystallized Bandelier pluton at about 4·7 km. Because this estimate accounts for post-eruption resurgence, the depth to the chamber before ignimbrite effusion should lie between 5 and 6 km. Various seismic experiments conducted since 1981 have identified low-velocity cylindrical bodies underlying the caldera that are attributed to residual magma in a large chamber [see discussion by Goff & Gardner (2007, p. 56)]. Steck *et al.* (1998) concluded that the minimum melt fraction in this residual chamber is roughly 13%, whereas Aprea *et al.* (2002) determined that the top of the present chamber is at 7 ± 1 km depth. Drilling of more than 40 geothermal wells inside the Valles Caldera to depths as great as 3·2 km has not encountered any crystallized sills, dikes, plugs, or other intrusive bodies beneath the resurgent dome (Goff & Gardner, 2007). Thus, drilling and seismic data limit the depth to the top of the crytallized Bandelier chamber to between 3·2 and 7 km. As a result, we believe that the pressure distribution in the magma chamber during eruption of the Tshirege can be confidently fixed at 200 ± 50 MPa.

METHODS

Sample collection

We conducted comprehensive sampling of the uppermost tephra units of the Cerro Toledo Formation east of the Valles Caldera [Units 7–14 of Stix (1989)], all subunits of the UBT as defined by Warren *et al.* (2007), including the Tsankawi Pumice Bed, the Deer Canyon Rhyolite and

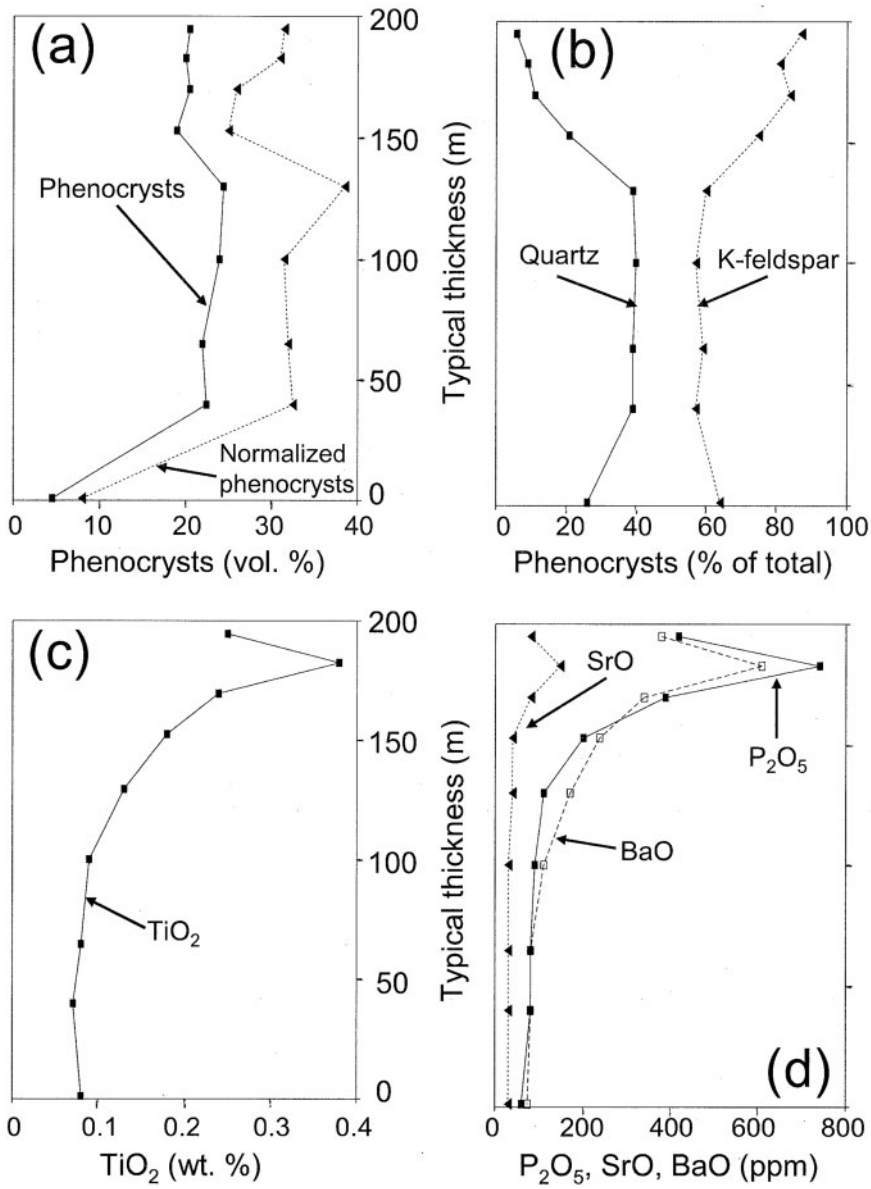

Fig. 2. Variation of typical flow unit thickness versus average values of selected phenocryst contents (a, b) and chemistry (c, d) using the comprehensive database of Warren *et al.* (2007). Flow unit naming scheme is from Warren *et al.* (2007) with modifications of Units 4 and 5 described by Goff & Warren (2010). More than 750 chemical analyses and 170 modal analyses confirm the vertical petrological and mineralogical gradients in the Tshirege Member ignimbrites documented years earlier (Smith & Bailey, 1966; Warshaw & Smith, 1988). 'Typical' flow unit thicknesses are for the Pajarito Plateau area WSW of the Valles Caldera (Warren *et al.*, 2007), but all researchers of the Tshirege have stated that thicknesses vary greatly depending on proximal and distal exposures relative to source, and on pre-existing topography. Upper flow units are more tongue-like than sheet-like owing to smaller erupted volumes and restricted eruption directions. There is no place where a complete section of all Tshirege flow units is exposed or drilled, even within the Valles Caldera (Warren *et al.*, 2007; Goff *et al.*, 2007).

Redondo Creek Rhyodacite resurgence-related lavas, and the first post-caldera moat rhyolite, Cerro del Medio (Table 2). This sample suite essentially covers the formation of the Valles Caldera, from pre-UBT volcanism, the entire UBT, resurgence-related lavas to ring fracture volcanism. We also sampled hornblende dacite pumices present within the Tsankawi Pumice Bed and unit 1g of the UBT at several locations (Table 2). Spatial variations in mineralogy, welding and crystallization of the UBT outflow sheets have produced numerous subunit classifications that differ from the original stratigraphy of Smith & Bailey (1966). The nomenclature applied in this study uses the subunits as originally defined by Broxton *et al.* (1995*a*, 1995*b*) and further constrained by Warren *et al.* (2007) for the upper

Fig. 3. Photograph of Tshirege Member, Bandelier Tuff, exposed in the north wall of Pueblo Canyon east of the Valles Caldera and the town of Los Alamos. Qts, Tsankawi Pumice Bed covered mostly by talus; Qbt1g, lower flow unit 1, primarily unaltered; vpn, vapor phase notch, a widespread stratigraphic marker; Qbt1v, upper flow unit 1, which displays extreme vapour phase (deuteric) alteration; Qbt2, flow unit 2; Qbt3, flow unit 3. Flow units 1 and 2 form roughly 70% by volume of the Tshirege Member (photograph by Fraser Goff).

ignimbrite sections (Fig. 1b). The latter study split unit 4 of Broxton *et al.* (1995*a*) into units 4 and 5, as this uppermost flow unit exhibits substantial geochemical, physical and spatial variation (Goff *et al.*, 2007; Goff & Warren, 2010).

The plinian Tsankawi Pumice Bed of the UBT was sampled at a roadcut ~8 km NW of the caldera at a location situated within the thickest accumulation of the Tsankawi deposit as indicated by the isopach mapping of Self *et al.* (1986) (Fig. 1a). UBT subunits were collected from both intra-caldera and extra-caldera locations (Table 2). Surface exposures of flow units underlying UBT subunit 4 are not recognized within the intra-caldera environment. Hence subunits 1–3t of the UBT were sampled from locations on the Pajarito Plateau, SE of the caldera. Samples of the Deer Canyon and Redondo Creek lavas and their associated tuffs were sampled from multiple locations on the resurgent dome, to ensure that we had samples from several vents to assess any spatial relationships (Fig. 1b).

Sample preparation

Single quartz crystals were handpicked following application of a light crush to a bulk sample. We used the sieved fraction (between −1 and 0·5 phi units) yielding the highest

Table 1: Comparative mineral abundance, oxygen fugacity, and temperature data, Tshirege Member, Bandelier Tuff

Flow unit identification		Selected average mineral abundances (% of total phenocrysts)						
Warren *et al.* (2007)	Warshaw & Smith (1988)	K-feldspar	Quartz	Orthopyroxene	Clinopyroxene	Fayalite	Magnetite	Ilmenite
Unit 5	Unit V	85·5, $n=17$	6·1, $n=17$	0·76, $n=12$	1·37, $n=12$	0·01, $n=16$	1·55, $n=17$	0·24, $n=17$
Unit 4u	Unit V	80·5, $n=7$	8·9, $n=7$	1·40, $n=5$	1·62, $n=5$	0, $n=5$	1·13, $n=7$	0·13, $n=7$
Unit 4l	Unit V	83·2, $n=10$	11·2, $n=11$	0·48, $n=6$	1·98, $n=6$	0, $n=9$	1·44, $n=10$	0·04, $n=9$
Unit 3t	not recognized	74·9, $n=20$	20·8, $n=22$	0·44, $n=12$	1·54, $n=12$	0·08, $n=14$	1·10, $n=22$	0, $n=22$
Unit 3	Unit IV	59·7, $n=58$	38·4, $n=58$	0·03, $n=50$	0·89, $n=52$	0·02, $n=54$	0·53, $n=29$	0, $n=29$
Unit 2	Unit III	57·6, $n=24$	40·2, $n=24$	0, $n=17$	0·74, $n=18$	0·27, $n=18$	0·52, $n=6$	0, $n=6$
Unit 1v	Unit II	58·9, $n=14$	39·5, $n=16$	0, $n=4$	0·95, $n=4$	0·23, $n=4$	0·21, $n=12$	0, $n=12$
Unit 1 g	Unit II	58·2, $n=14$	39·8, $n=16$	0, $n=6$	0·96, $n=6$	0·28, $n=8$	n.d.	n.d.
Unit 1 g	Unit II	63·7, $n=4$	31·8, $n=4$	0, $n=3$	1·69, $n=3$	0, $n=3$	0·3, $n=10$	0, $n=10$
Tsankawi	Unit I							

Flow unit identification		Oxygen fugacity $\log_{10}fO_2$	T (°C) Fe–Ti oxide	T (°C) Magnetite–fayalite	T (°C), two pyroxenes	
Warren *et al.* (2007)	Warshaw & Smith (1988)				Clino-pyroxene	Ortho-pyroxene
Unit 5	Unit V	−13·01	837		840	770
Unit 4u	Unit V					
Unit 4l	Unit V					
Unit 3t	not recognized					
Unit 3	Unit IV				785	810
Unit 3	Unit IV				760	800
Unit 2	Unit III	−15·54		753		
Unit 2	Unit III	−15·70		746	700	800
Unit 1	Unit II	−16·20		726		
Unit 1	Unit II	−16·57		710		
Unit 1	Unit II	−16·69		706		
Tsankawi	Unit I	−16·90	697			

Mineral contents are from Warren *et al.* (2007); oxygen fugacity and temperature data are from Warshaw & Smith (1988). [Note the differences in flow unit naming schemes, a problem that has plagued research on the Tshirege Member for years (see Broxton & Rogers, 2007).] *n*, number of thin sections; n.d., not determined.

return of complete, undamaged crystals. Quartz crystals were mounted in epoxy within 1 inch grain mounts. This technique was used for CL imaging and laser ablation inductively coupled plasma mass spectrometry (LA-ICP-MS) analysis of quartz grains from Cerro Toledo Formation (CTF) units 7–14, the Tsankawi Pumice Bed, UBT Unit 1 g and Cerro del Medio. We used polished thin sections for the remaining units. Two hornblende dacite pumices were first cleaned with deionized water, dried for 72 h and the weathered outer surface removed with a rotary grinder to eliminate any erroneous data prior to X-ray fluorescence (XRF) analysis for major and trace elements.

Cathodoluminescence imaging

CL analysis of quartz crystals in thin section and grain mounts was performed using a Reliotron® III cold-cathode unit mounted on a Leitz petrographic microscope stage. Beam voltages ranged from 6·5 to 7·0 kV at 0·5 mA current and 6 Pa operating pressure. The voltage was increased to resolve numerous thin oscillatory zones, which may not be apparent at lower voltages. Once a stable beam was obtained, the beam was focused, reducing the width to ~2 mm, which was sufficient to excite most quartz samples. For a circular beam on a quartz of 1 mm diameter, the calculated beam power density was ~420 W cm^{-2}.

Table 2: Sampling localities and descriptions for units in this study

Sample no.	Sample ID	Formation or Member		Subunit	Description	US UTM reference, 13 S	
						Northing	Easting
16	JW08-22	Qvvf	Cerro del Medio Member	Unit South	Rhyolite lava	N3970842	E370034
15	JW08-04	Qrc	Redondo Creek Member	Central dome	Rhyodacite lava	N3973735	E358532
14	JW08-05	Qdc	Deer Canyon Member	Central dome	Rhyolite lava	N3974052	E359678
13	JW08-01			Western dome	Porphyritic rhyolite lava	N3971203	E354802
12	JW08-08c	Qbt	Upper Bandelier Tuff (Tshirege Member)	Unit 5u intracaldera	Moderately welded ignimbrite, prominent crystal-rich flattened pumices	N3966059	E378527
11	JW08-23			Unit 5u extracaldera	Partially welded to vitrophyric ignimbrite	N3972515	E356475
10	JW08-08g			Unit 4u intracaldera	Intracaldera moderately welded, devitrified ignimbrite	N3972487	E356499
9	JW08-17			Unit 4l extracaldera	Non-welded to densely welded, devitrified ignimbrite	N3973027	E379996
8	JW08-11			Unit 3t	Moderately welded to densely welded ignimbrite	N3965596	E376673
7	JW08-26			Unit 3	Non-welded to partially welded vapour phase-altered ignimbrite	N3970393	E383549
6	JW08-25			Unit 2	Poorly sorted, vapour phase-altered ignimbrite	N3969621	E385906
5	JW08-24HD			Hornblende dacite pumice	Single (<10 cm) distinctive light grey pumices within Unit 1g		
4	JW08-24			Unit 1g	Non-welded, poorly sorted vitric ignimbrite		
3	JW08-15J			Hornblende dacite pumice	Single (<10 cm) distinctive light grey pumices within Tsankawi	N3984712	E347118
2	JW08-15			Tsankawi Pumice Bed	Massive lapilli pumice bed, 8 km NW of caldera		
1	JW08-27	Qct	Cerro Toledo Formation	Upper pumice bed (7–14)	Massive lapilli pumice bed underlying UBT	N3970682	E387836

Sample number corresponds to localities depicted in Fig. 1a and b. GPS coordinates acquired using NAD27 datum. Cerro Toledo Formation Units 7–14 as described by Stix (1989).

A QImaging® Retiga EXi camera oriented vertically down the microscope objective provided digital colour images at a spatial resolution of 6·45 μm. Image acquisition times varied depending upon the CL intensity but were generally in the range of 5–30 s. Once a desirable exposure time was calibrated for each sample, successive images used the same exposure time to maintain experimental reproducibility. Post-capture image processing was performed with Adobe Photoshop® to increase the brightness and contrast of zoned quartz grains and to highlight any low-contrast diffuse zones. No colour adjustment was made to any image.

Laser ablation inductively coupled plasma mass spectrometry

Titanium concentrations in quartz crystals were obtained using a New-Wave UP-213 nm laser ablation system attached to a Perkin Elmer/SCIEX ELAN 6100 DRC plus ICP-MS system at McGill University. Experiments were conducted as either (1) spot analyses to resolve different compositional zones or (2) line scans to traverse zone boundaries, both at 10 Hz and ~10 J cm^{-2} laser fluence. Beam sizes for each method ranged from 40 to 60 μm, depending upon the thickness and friability of the quartz crystals. We took care to avoid melt inclusions, which have high Ti concentrations relative to the quartz. Data reduction, including signal selection and background count determination, was performed with GEMOC 'Glitter' software.

Two isotopes of titanium were chosen for this study. The greater abundance of ^{48}Ti (73·8 %) over ^{49}Ti (5·5 %) results in higher count rates for the former isotope, hence this isotope was chosen as most representative. In addition, ^{29}Si was selected as an internal reference isotope, with ^{27}Al, ^{43}Ca and ^{96}Zr monitored to identify melt inclusions, crystallographic defects or surface contamination.

To resolve an isobaric interference of Ca on ^{48}Ti, benitoite ($BaTiSi_3O_9$), a calcium-free titanium silicate, was used as the primary standard. To compare multiple sessions, a pooled average of ^{48}Ti concentrations and a pooled standard deviation were calculated. The pooled standard deviation (S_p) is defined by

$$S_p = \sqrt{\frac{(n_1-1)s_1^2 + (n_2-1)s_2^2 \cdots + (n_k-1)s_k^2}{n_1 + n_2 \cdots + n_k - k}} \quad (1)$$

where n_1 is the number of analyses of the first session, s_1 is the standard deviation of that session and k is the overall

number of sessions being combined. The pooled standard deviation yields an overall error of 7·3% (RSD) relative to the ideal stoichiometric Ti in benitoite, and 7·2% (RSD) relative to the pooled average concentration. Low-Ti, unzoned quartz from the Tsankawi Pumice Bed was also analysed periodically to assess reproducibility at low Ti concentrations (20–30 ppm). Two crystals that were periodically analysed yielded precisions of 3·97% and 5·19%, respectively (see Supplementary Data Table 1, available for downloading at http://www.petrology.oxfordjournals.org). The limit of quantification of the LA-ICP-MS system is ≤2 ppm Ti and the detection limit is <1 ppm Ti, based on Poisson background count statistics.

Electron microprobe

We used the electron microprobe to determine Ti concentrations in melt inclusions in quartz crystals and matrix glasses adhering to the crystals (see Supplementary Data Table 2). Glass analyses were performed using a JXA JEOL 8900 L electron microprobe at McGill University. Operating conditions included a defocused beam of 20 μm diameter, 15 kV voltage, and 20 nA current. The microprobe was optimized for Ti in particular, an element that is not affected by sodium migration (Morgan & London, 2005). Count times for major elements (Si, Al, Fe, Mn, Mg, Na, K) were 20 s. The count time for Ti was extended to 100 s to improve statistical precision. Standardization was performed on homogeneous Yellowstone rhyolite glass (for Na, Al, K, Si) and two basaltic glasses, BMAK (Ti) and BIND (Fe, Mg, Ca), which are international standards from the Smithsonian Institution (Jarosewich *et al.*, 1980). The relative standard deviation for Ti in the BMAK glass standard was 0·8%, and analyses showed excellent accuracy and precision for an external standard (UTR-2, Stix *et al.*, 1995) that was analyzed repeatedly (within 0·01 wt %, Supplementary Data Table 1). Prior to analysis, we took care to identify areas of homogeneous glass that were free from microlites and surface contamination. For the Tsankawi Pumice Bed, we analysed glass adhering to single quartz crystals in addition to melt inclusions from each respective crystal. All melt inclusions were 100% glassy with no associated bubbles, cracks, or daughter crystals. The reader is referred to Stix & Layne (1996) for further details on the glasses.

X-ray fluorescence

A Phillips PW2440 4 kW spectrometer at the McGill University Trace Element Analytical Laboratories was used to acquire major element (Si, Ti, Al, Fe, Mn, Mg, Ca, Na, K, P) and trace element (Nb, Rb, Sr, Th, Y, Zr) analyses of several glass separates from the Cerro Toledo Formation and two bulk hornblende dacite pumices from UBT Unit 1 g. All major and trace elements were acquired using 32 mm diameter fused beads. Two natural rhyolitic glasses, UTR-2 and NBS-278 (Gladney & Bower, 1985; Stix *et al.*, 1995), were used as reference materials, both yielding excellent experimental reproducibility (Supplementary Data Table 1).

RESULTS

Quartz CL zoning patterns

A total of 224 quartz crystals and fragments were characterized for their respective CL zonation patterns following classifications used by Peppard *et al.* (2001; see their fig. 11a and b) for quartz from the Bishop Tuff, erupted from the Long Valley caldera.

Figures 4 and 5 show the zoning classifications applied in this study. Type 1 zoning represents quartz crystals with low-intensity CL cores overgrown by a high-intensity CL rim, or in some cases, multiple high-intensity CL rims. Type 2 zoning represents quartz crystals with a high-intensity CL core and low-intensity CL rim. Type 3 was used to classify unzoned quartz crystals. The Type 1 classification was further subdivided (1a–1d) to account for multiple zones of varying CL intensity and the nature of the core–rim boundary, whether diffuse or sharp (Figs 4 and 5). All samples displayed variable blue to violet CL colours and also exhibited time-dependent loss of the blue emission wavelength within ~30 s of irradiation, gradually reverting to an underlying red CL colour (e.g. Peppard *et al.*, 2001; Müller *et al.*, 2002; Götze *et al.*, 2005). This phenomenon was particularly noticeable within quartz of the upper Cerro Toledo Formation and Tsankawi Pumice Bed units. It is of note that these quartz crystals were not zoned prior to wavelength emission loss.

The Valles Caldera sample suite used for this study is characterized by four distinct variations in the nature of CL zoning with respect to stratigraphic position. Figure 6 depicts the quantitative abundance of each quartz zoning type for the various units.

Upper Cerro Toledo Formation and early UBT (Tsankawi, UBT units 1g and 2)

Figure 6 shows a predominance of unzoned quartz crystals (Type 3, Figs 4 and 5) within the upper Cerro Toledo Formation [Units 7–14 of Stix (1989)], the Tsankawi Pumice Bed and units 1 g and 2 of the UBT. A minor population of quartz exhibits fine-scale (<10 μm) oscillatory zones, characterized by alternating bands of high and low CL intensity. Additionally, unit 2 contains several normally zoned quartz crystals (Type 2), whereby the core region exhibits increased CL intensity relative to the lower-intensity rim. The quartz of the Tsankawi Pumice Bed is characterized by ubiquitously distributed melt inclusions, which induce local areas of increased CL emission, but this enhanced CL emission is not representative of primary quartz growth zones. We note the predominance

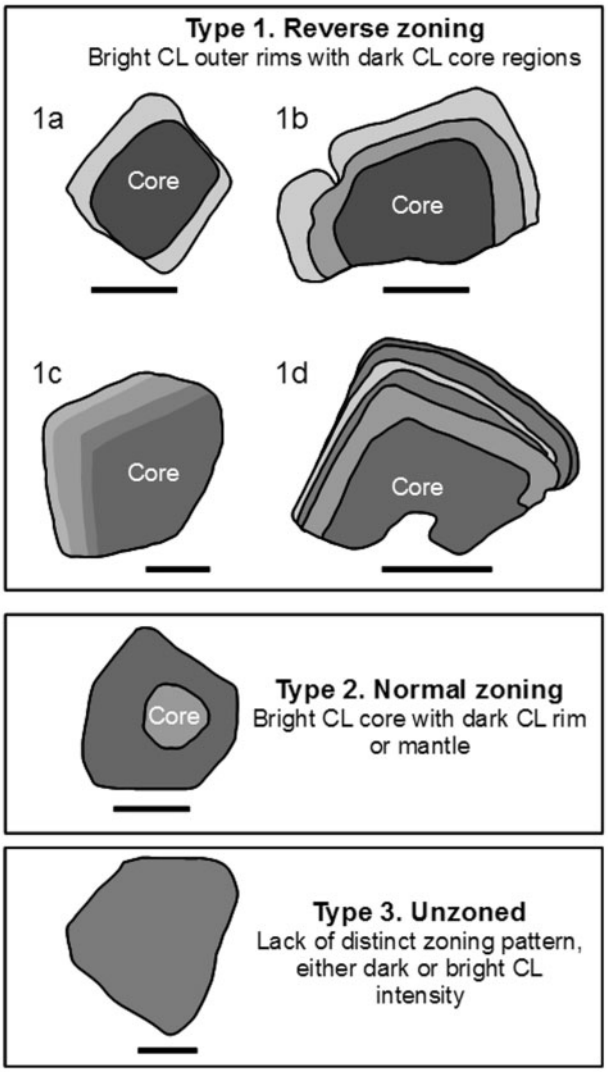

Fig. 4. Quartz cathodoluminescence (CL) zoning pattern classifications following the terminology of Peppard *et al.* (2001). Grayscale represents the CL signal; lighter shades are higher intensity and thus higher Ti. The zones shown for the crystal depicted in 1c have diffuse boundaries that create a gradation in CL intensity from core to rim. Scale bars represent 0·5 mm.

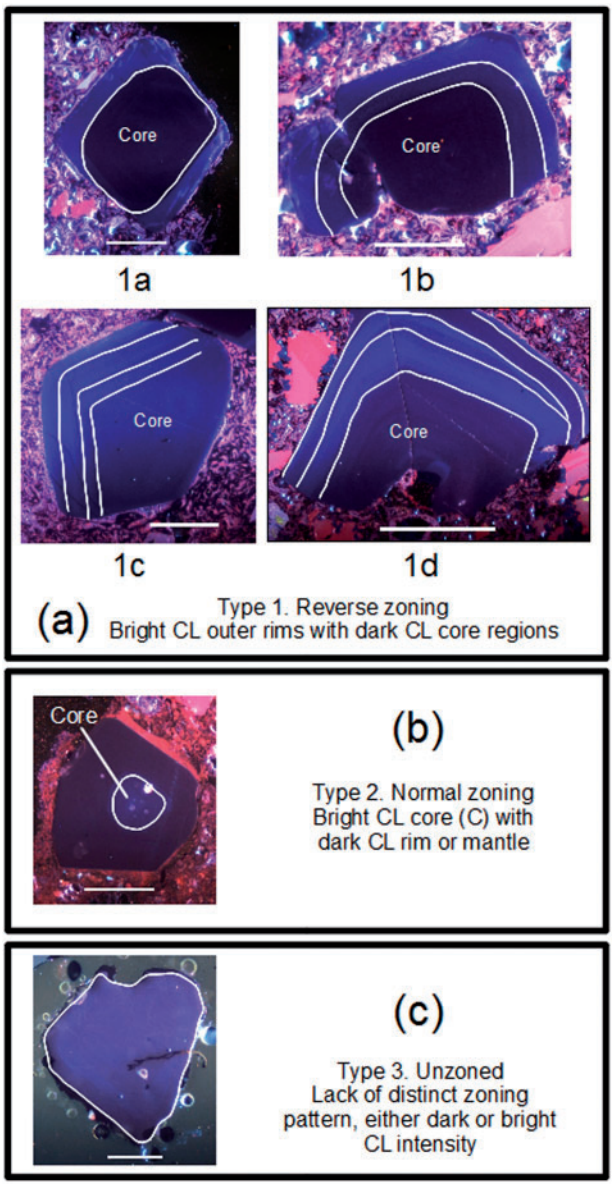

Fig. 5. Quartz cathodoluminescence (CL) zoning pattern classifications following the terminology of Peppard *et al.* (2001). White lines define zone boundaries where applicable. (a) Type 1, reverse zoning. (b) Type 2, normal zoning. (c) Type 3, unzoned. All scale bars represent 0·5 mm.

of small, 50–100 μm embayments and the rounded morphology of most quartz crystals within these early erupted units. Together these units represent about 70% of the total erupted volume of the UBT.

Mid-to-late erupted UBT (ignimbrite units 3–5)

By contrast, quartz crystals from the mid-to-late erupted ignimbrite units (UBT 3, 3t, 4 and 5) show dominantly Type 1 zoning (82–95% abundance). There is a low abundance (5–15 %) of Type 3, unzoned quartz (Fig. 6). Zone boundaries within zoned quartz crystals are commonly sharp and concordant, particularly within units 3 and 3 t, with zone boundary thicknesses for unit 3 averaging 28·5 μm. The quartz crystals from these units are also sometimes characterized by 100–200 μm thick zones of intermediate CL intensity situated between the core and rim and separated by sharp, concordant boundaries. The variation in Type 1 zoning (i.e. relative proportions of Type 1a, 1b, 1c and 1d) is relatively uniform for the mid-to-late UBT units.

Deer Canyon Rhyolite

The resurgence-related Deer Canyon Rhyolite exhibits variation in CL zoning in terms of its spatial distribution

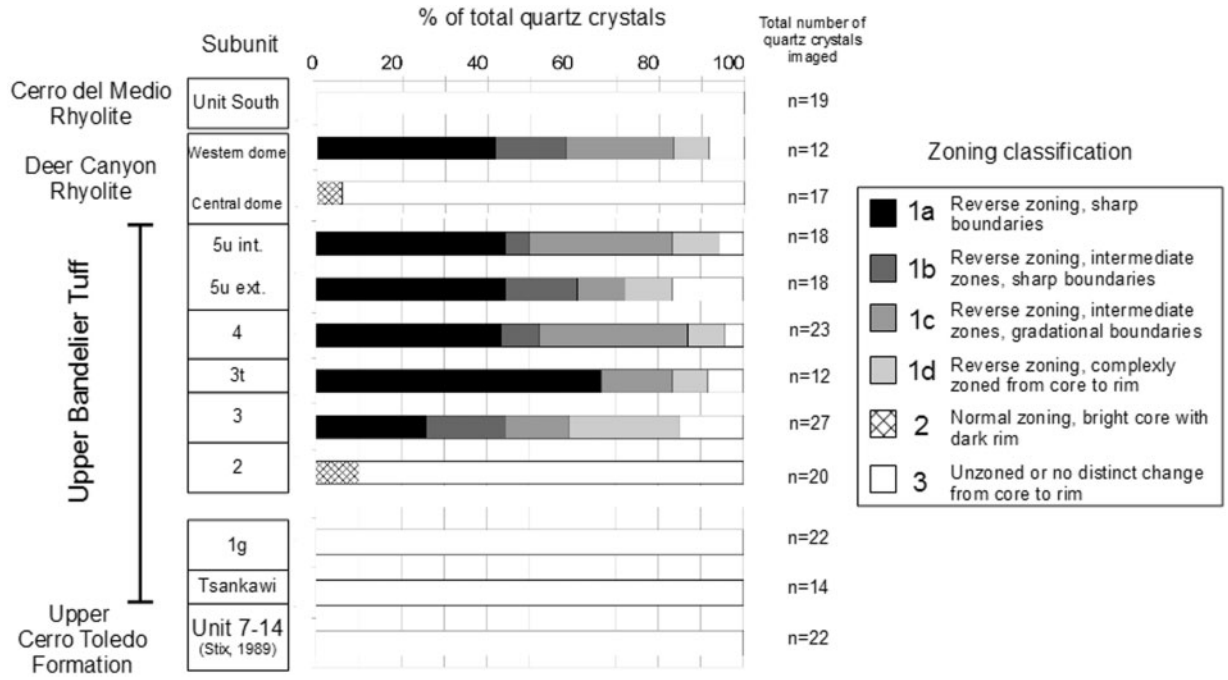

Fig. 6. Quartz cathodoluminescence zoning patterns correlated to stratigraphic position. Subclassifications follow the terminology of Peppard *et al*. (2001). Subunit 1v of the UBT was not sampled for this project. The lack of quartz in the Redondo Creek Rhyodacite prevented CL analysis for this unit. int, intracaldera setting; ext, extracaldera setting.

on the resurgent dome, although our two samples are derived from the same mapped stratigraphic unit. Porphyritic rhyolite sampled from the western resurgent dome (sample 13, Fig. 1b) has quartz crystals that are both reversely zoned (90% abundance) and unzoned (10% abundance). Zone boundaries range from sharp and concordant to diffuse. Intermediate zone widths range from 180 to 300 μm, some showing complex cross-cutting relationships. Embayments are ubiquitous for almost all zoned quartz grains, although distinguishing the temporal relationship between dissolution and rim growth is difficult to reconcile given the resolution of our images. Preliminary observations suggest that dissolution may have occurred prior to growth, as thin (<20 μm) zones of high CL intensity commonly surround embayments (see Fig. 7c, inset). The melt inclusions are confined to core regions, and the sharp CL boundaries imply growth of the outer rims shortly before eruption. We also sampled Deer Canyon Rhyolite from a central resurgent dome location (sample 14, Fig. 1b). The range of crystal size here is greater (0·5–2·85 mm) than for the porphyritic sample, exhibiting no dominant crystal size. Excluding two normally zoned quartz grains, all crystals are unzoned, rounded and/or embayed (Fig. 6). Synneusis texture (Vance, 1969) of the smaller quartz grains and feldspar grains in this sample stands in pronounced contrast to the large 2–3 mm diameter quartz crystals from the porphyritic sample.

Cerro del Medio Rhyolite

CL analysis of quartz from the Cerro del Medio ring fracture rhyolite marks a return to dominant Type 3 zoning with unzoned, small (0·5–1·0 mm), rounded quartz phenocrysts (Fig. 6). Unit South represents the most crystal-rich sample of the Cerro del Medio complex (5 vol. %) (Fig. 1b; Gardner *et al*., 2007). Under bombardment by the electron beam, we did not witness the high degree of short-lived blue CL emission prevalent with quartz from the upper Cerro Toledo Formation and Tsankawi Pumice Bed.

In summary, we note (1) the abrupt occurrence of zoned quartz crystals commencing within unit 3 of the UBT ignimbrite and (2) variation of CL zoning in quartz from the resurgence and ring fracture volcanic rocks (Fig. 6). The corresponding titanium-in-quartz concentrations discussed below are closely linked to observed CL zoning.

Ti concentrations in quartz

We analysed 130 quartz crystals that had been previously characterized for their CL zonation patterns. A number of interesting trends emerge, and in this section we correlate the titanium values to the CL zonation patterns. Comprehensive results for Ti-in-quartz are reported in Supplementary Data Table 3 and plotted collectively in Fig. 8. Table 3 summarizes the Ti-in-quartz measurements.

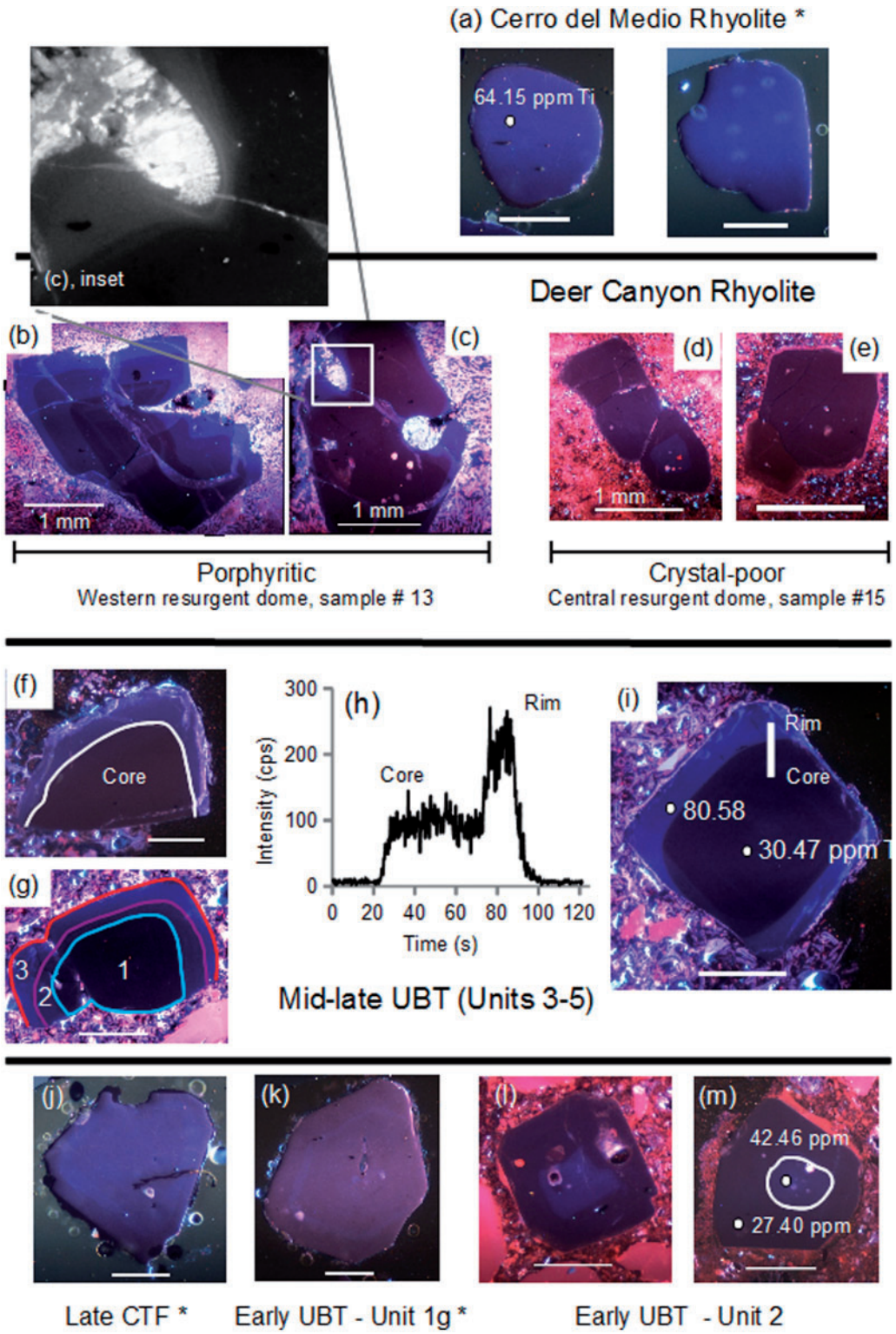

Fig. 7. Mosaic of characteristic CL zoning patterns in quartz crystals with respect to stratigraphic position. All scale bars represent 500 μm unless otherwise stated. The symbol * indicates a quartz crystal imaged in a grain mount. CL analysis reveals predominantly zoned (low-intensity core and high-intensity rim) quartz within the mid–late UBT ignimbrite units and porphyritic Deer Canyon Rhyolite. Average titanium concentrations (ppm) determined from LA-ICP-MS analyses are given for core and rim regions. (a) Unzoned quartz crystal with a high-intensity CL signal, characteristic of quartz crystals from Cerro del Medio flow unit South, sample 16. (b) Large (~3 mm) zoned quartz

(continued)

Because we are dealing with grouped data, it is useful to consider two important statistics. First, the pooled average concentration ($\bar{X}_T$) was calculated using the relation

$$\bar{X}_T = \frac{\left[\left(\bar{X}_A \cdot \mathcal{N}_A\right) + \left(\bar{X}_B \cdot \mathcal{N}_B\right) \cdots + \left(\bar{X}_n \cdot \mathcal{N}_n\right)\right]}{\left(\mathcal{N}_A + \mathcal{N}_B \cdots + \mathcal{N}_n\right)} \quad (2)$$

where $\bar{X}_A$ is the average concentration of the first group and $\mathcal{N}_A$ is the number of samples in that group. Second, a pooled standard deviation (S_T) is calculated by

$$S_T = \sqrt{\frac{\left[\mathcal{N}_A\left(\bar{X}_A \cdot \mathcal{N}_A\right) + \mathcal{N}_B\left(\bar{X}_B \cdot \mathcal{N}_B\right) + \cdots + \mathcal{N}_n\left(\bar{X}_n \cdot \mathcal{N}_n\right)\right]}{\mathcal{N}_A + \mathcal{N}_B + \cdots + \mathcal{N}_n} - X_T^2} \quad (3)$$

where $\mathcal{N}_A$ is the number of samples, $\bar{X}_A$ is the average concentration and s_A is the standard deviation of the group. Equations (2) and (3) are from Downie & Heath (1970). We underline the fact that the analytical error on our Ti-in-quartz measure measurements is 7·3% (RSD).

Upper Cerro Toledo Formation and early UBT (units 1g and 2)

The unzoned quartz crystals of the upper Cerro Toledo Formation, the Tsankawi Pumice Bed and units 1g and 2 of the UBT fall within a small range of 24–33 ppm Ti. The pooled average concentration and standard deviation are 27·82 ± 2·25 ppm Ti (Table 3). The two outlier core Ti values of 42 ppm and 56 ppm Ti for UBT unit 2 correspond to high-intensity CL core regions that are overgrown by rims of lower CL intensity and lower Ti content, referred to as normal zoning (Fig. 8).

Mid-to-late erupted UBT (units 3–5)

The abrupt appearance of dominant Type 1 CL zoning (low-intensity core with high-intensity CL rim overgrowths) within UBT unit 3 (Fig. 6) is reinforced by large core-to-rim increases in titanium within all zoned quartz. Core values are similar to those in quartz from the preceding units, falling within a relatively narrow range of 25–45 ppm Ti. The pooled average concentration and standard deviation are 31·37 ± 4·71 ppm Ti (Table 3). A normally zoned quartz crystal (high-intensity cores and low-intensity CL rims) from unit 3 plots with a high core Ti value reflected in the outlier in Fig. 8. Similarly, the outlier value of 70 ppm Ti for UBT unit 5u represents a high-intensity CL unzoned quartz crystal.

Throughout units 3–5 of the UBT, outer rims show a 20–70 ppm increase in Ti with respect to core values. The range of rim concentrations is largest within UBT unit 3 (43–103 ppm Ti). Conversely, the smallest range of rim Ti values is seen for unit 3t (76–93 ppm Ti). The maximum rim concentration analysed was 104 ppm Ti from UBT unit 5u, and the minimum rim value was 43 ppm Ti from a complexly zoned quartz crystal with diffuse zone boundaries from UBT unit 3 (Table 3). The highest average rim concentration is calculated for quartz of UBT unit 3t (82 ppm), and the lowest for UBT unit 4u (63 ppm). Zones of intermediate CL intensity also exhibit Ti concentrations that are transitional between core and rim values. Rim Ti concentrations of quartz from UBT units 3–5 are 71 ± 9 ppm when a pooled average concentration and standard deviation are considered (Table 3).

Deer Canyon Rhyolite

Cores of Deer Canyon Rhyolite quartz crystals for both the western porphyritic sample [DC (P) in Fig. 8] and the central resurgent dome sample (DC in Fig. 8) show titanium concentrations similar to those in quartz cores from the upper CTF and UBT. These fall within a range of 25–35 ppm Ti. The outlier core value for the DC sample represents a high-intensity CL core of a normally zoned, Type 2 quartz crystal.

The porphyritic Deer Canyon Rhyolite sample containing zoned quartz exhibits quartz rim concentrations ranging from 51 to 89 ppm Ti, similar to the range of concentrations of quartz rims from units 3–5 of the UBT (Table 3). The CL zoning variation between the two Deer Canyon samples is thus also reflected in compositional differences.

Cerro del Medio Rhyolite

The unzoned Cerro del Medio quartz samples have Ti contents that are generally similar and overlap with the rim concentrations of UBT units 3–5 and the porphyritic Deer Canyon Rhyolite sample. Ti concentrations are grouped within a range of 60–74 ppm (Table 3).

In summary, all unzoned quartz and core regions of zoned quartz, excluding Cerro del Medio, fall within a

Fig. 7 Continued
crystal from the porphyritic Deer Canyon Rhyolite from the western resurgent dome. (c) A quartz crystal from the same unit exhibiting several embayments. (c, inset) A monochrome enlargement of a high-intensity CL rim following a pre-existing embayment. (d) Synneusis texture (crystal attachment) of three quartz crystals from the crystal-poor Deer Canyon Rhyolite from a central resurgent dome location. The crystal at the bottom of the image exhibits Type 2, normal zoning. (e) Unzoned quartz crystal from the same Deer Canyon Rhyolite sample. (f) Reversely zoned quartz crystal from UBT unit 3, showing a high-intensity CL rim and resorbed, low-intensity CL core. (g) Zoned quartz grain from UBT unit 3 exhibiting (1) low-intensity CL core and (3) high-intensity CL rim, separated by a zone of intermediate CL intensity (2). (h) Raw count rates during line scan (core–rim) of a zoned quartz crystal (i), passing through a sharp zone boundary. The abrupt signal increase, indicative of a ~50 ppm increase in Ti from core to rim, should be noted. (j) Unzoned quartz crystal from the upper Cerro Toledo Formation. (k) Unzoned quartz crystal from early erupted UBT unit 1g. (l) Normally zoned quartz crystal from UBT unit 2. (m) A normally zoned (Type 2) quartz crystal from UBT unit 2 showing corresponding titanium concentrations of core and rim.

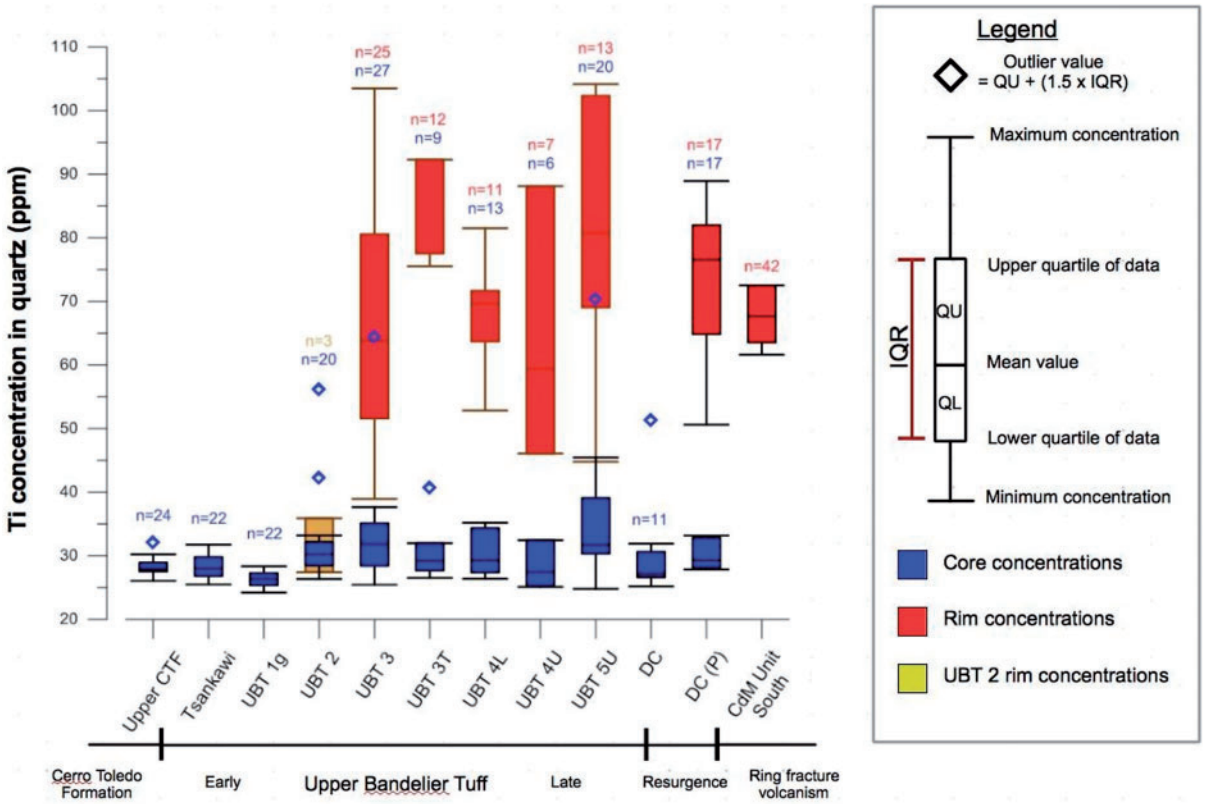

Fig. 8. Box–whisker plot showing the results of LA-ICP-MS analysis of quartz cores and rims with respect to stratigraphic position. DC (P), porphyritic Deer Canyon Rhyolite sampled from the western resurgent dome; DC, Deer Canyon Rhyolite sampled from the central resurgent dome; CdM, Cerro del Medio moat rhyolite. The plot is constructed to show the spread of titanium data as defined by the maximum, minimum, lower and upper quartiles and mean concentration. The number of analyses (*n*) on cores and rims is shown for each unit. Outlier values, represented by open diamond symbols, are calculated as 1·5 times the inter-quartile range plus the value of the upper quartile of the dataset (see legend).

Table 3: Summary of Ti-in-quartz concentrations of single eruptive units and grouped statistics, correlated to stratigraphic position

Sample no.	Formation or Member	Subunit	Ti-in-quartz concentrations (ppm)						Pooled average (ppm)		Pooled standard deviation (ppm)	
			Core Average	Core Min.	Core Max.	Rim Average	Rim Min.	Rim Max.	Core	Rim	Core	Rim
16	Qvvf	Cerro del Medio Unit South	64·09	60·42	72·54							
13	Qdc	Deer Canyon Member Western resurgent dome	30·28	27·72	34·89	70·69	50·65	88·94				
14	Qdc	Deer Canyon Member Central resurgent dome	28·40	25·20	31·92							
12	Qbt	UBT Unit 5u intracaldera	32·06	24·80	39·87	80·23	44·80	104·17				
11		UBT Unit 5u extracaldera	34·00	29·12	45·45	75·84	58·29	84·44				
10		UBT Unit 4u intracaldera	27·82	25·11	32·46	63·25	46·08	88·11	31·37	70·82	4·71	8·58
9		UBT Unit 4l extracaldera	30·76	26·39	35·19	68·19	52·85	81·53				
8		UBT Unit 3t	31·99	26·54	40·80	81·64	75·53	92·67				
7		UBT Unit 3	31·41	25·44	37·66	64·21	42·97	103·53				
6		UBT Unit 2	29·97	26·37	33·20							
4		UBT Unit 1g	26·33	24·22	28·34				27·82		2·25	
2		Tsankawi Pumice Bed	28·02	25·48	31·76							
1	Qct	Upper CTF (Units 7–14)	28·30	26·08	31·12							

range of 24–45 ppm Ti. The abrupt occurrence of zoned quartz crystals commencing at UBT unit 3 (Fig. 6) is reflected by 20–70 ppm increases in rim Ti concentrations compared with core values. Quartz from the porphyritic Deer Canyon Rhyolite exhibits rim Ti concentrations similar to those of rims of zoned quartz from the mid-to-late erupted UBT. The central Deer Canyon sample exhibits quartz with Ti concentrations similar to those of the cores of UBT quartz.

Ti concentrations in glass

Titanium concentrations within glass of the plinian Tsankawi Pumice Bed, UBT units 1g, 4u and 5u, and the Redondo Creek Rhyodacite show an almost threefold increase with respect to decreasing eruption age (Supplementary Data Table 2). A total of 14 melt inclusions with an average of 293 ± 2 ppm Ti and 20 samples of adhering glass on Tsankawi quartz with an average of 308 ± 2 ppm Ti are virtually indistinguishable with respect to Ti concentrations. Analysis of homogeneous glass in UBT units 1g, 4u and 5u shows average concentrations of 560 ± 4, 814 ± 6 and 938 ± 7 ppm Ti, respectively. The Redondo Creek Rhyodacite sample yields a glass concentration of 915 ± 7 ppm Ti (Supplementary Data Table 2). In summary, there is a clear increase in Ti concentration in homogeneous glass upsection in the UBT and resurgent dome rhyolite stratigraphy.

Bulk analysis of several flow units of the Cerro del Medio Rhyolite complex gives Ti values of 622 ± 110 ppm (Gardner *et al.*, 2007; Supplementary Data Table 2). The low crystal content (<5% phenocrysts) of these lavas indicates that this value is generally representative of glass concentrations. Thus, Ti in glass decreases for the Cerro del Medio eruption cycle.

Hornblende dacite pumices

Samples of hornblende-bearing dacite pumice (HbDP) were obtained from the Tsankawi Pumice Bed and UBT unit 1g (Table 2). The pumices are light grey, finely porphyritic and vesicular, with visible hornblende crystals. The pumices range in diameter from 1 to 10 cm, with most ~2 cm. Following Stimac *et al.*, (1996), we note the occurrence of both phenocrysts and a xenocrystic component set within a finely vesicular glassy matrix containing ~70% microlites. Reacted xenocrysts of alkali feldspar crystals show sieve-textured cores and a large grain size (~3 mm) whereas the phenocrysts (plagioclase, two pyroxenes, hornblende, biotite, and Fe–Ti oxides) are generally euhedral, 0·5–1·0 mm in size, and form crystal aggregates. Both major and trace element compositions of the two pumices from UBT Unit 1g agree well with published values (see Supplementary Data Table 4; Self *et al.*, 1986; Balsley, 1988; Stix *et al.*, 1988; Stimac *et al.*, 1996). All are dacitic (67–69 wt % SiO_2), but show appreciable variation in trace element chemistry, notably Sr, Zr and Ba.

Temperature differences between cores and rims of quartz crystals

Using the Ti contents in quartz as measured by LA-ICP-MS, we can calculate temperature differences between the cores and rims of quartz crystals erupted in units 3, 4, and 5 of the UBT. For the cores, we use the average Ti concentrations found in the Tsankawi Pumice Bed and units 1g and 2 of the UBT. For the rims, we use the average Ti concentrations determined for each of units 3, 4 and 5. We calculate temperature differences by the approach of Huang & Audétat (2012) at 200 MPa pressure, as this pressure is well constrained for the Bandelier magma chamber during formation of the Valles Caldera, as summarized above. We also attempted to calculate temperatures at 200 MPa using the approach of Thomas *et al.* (2010), but all temperatures calculated by this method for the Tsankawi Pumice Bed, unit 1g, and unit 2 were below the water-saturated solidus at this pressure (Johannes & Holtz, 1996), and hence were unrealistic (the maximum calculated temperature was 595°C). In our calculations, we use four estimates of TiO_2 activity: (1) the *TitaniQ* geothermometer of Wark & Watson (2006); (2) the rutile saturation model developed by Hayden & Watson (2007); (3) a constant TiO_2 activity of 0·5, a value shown to be reflective of high-silica rhyolite systems [for comparison, Wark *et al.* (2007) and Wiebe *et al.* (2007) used a value of 0·6]; (4) the MELTS algorithm (Ghiorso & Sack, 1995; Asimow & Ghiorso, 1998; Gualda *et al.*, 2012). Details of the calculations can be found in Supplementary Data Tables 2 and 5 and Supplementary Explanatory Text 1. Temperature differences using rutile saturation TiO_2 activity and constant 0·5 TiO_2 activity are similar, with ranges of 102–140°C and 93–124°C, respectively. By contrast, temperature ranges using *TitaniQ* and MELTS TiO_2 activities are about half of the above values, with 56–75°C for *TitaniQ* and 35–69°C for MELTS. Integrating these data, it appears that temperatures were increased, on average, by at least ~35–140°C between the times when the quartz cores and rims crystallized (Fig. 9).

There are sometimes fine-scale zoning patterns present in Type 3 crystals, which could not always be resolved with our CL instrument. Such fine-scale zones consist of subtle changes in CL intensity, which translate into small differences in Ti concentration of the order of a few parts per million as measured by our LA-ICP-MS analyses. For example, a difference of 3 ppm Ti between two adjacent zones indicates a temperature difference of ~10°C calculated by the Huang & Audétat (2012) method using a nominal temperature of ~660°C and a TiO_2 activity of 0·5 (Wark & Watson, 2006). The temperature difference becomes only ~5°C at 780°C. Such temperature fluctuations imply small thermal variations in the shallow magma chamber during quartz crystallization and/or boundary layer effects. If the system was in a state of convection,

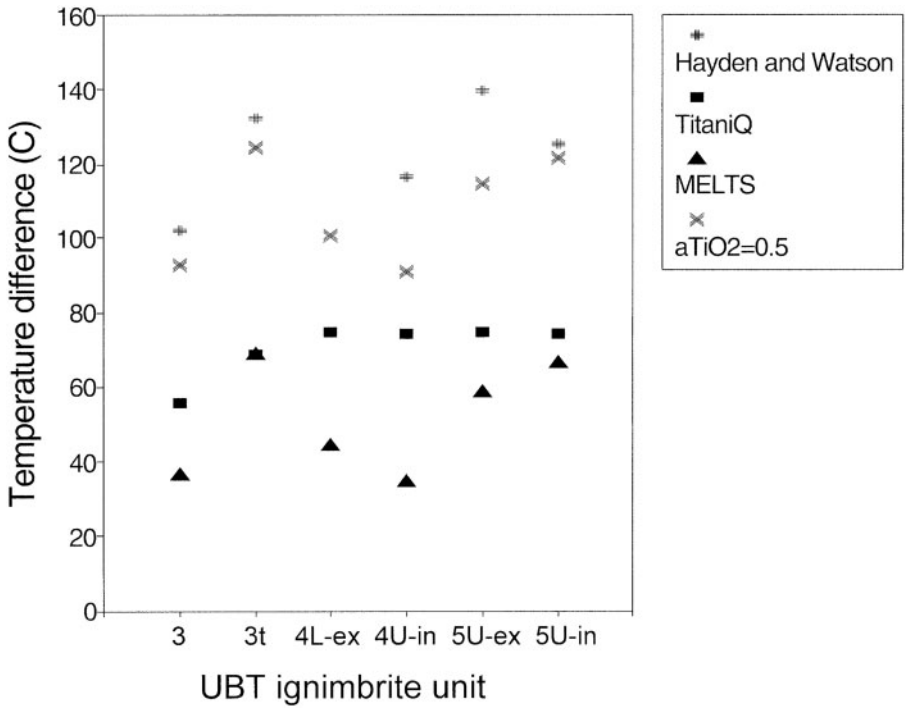

Fig. 9. Calculated temperature differences between the low-titanium cores and high-titanium rims of UBT units 3 to 5U. The temperature differences plotted are relative to the average calculated temperature of the combined Tsankawi pumice, UBT 1g and UBT 2, which represent 70% of the erupted volume of the UBT. Temperatures were calculated using the *TitaniQ* expression of Huang & Audétat (2012) with four methods of estimating TiO_2 activities in the melt. (See text for details.)

quartz crystals may have grown initially in deeper, hotter regions, then were remobilized to shallower, cooler zones. Another possibility is that quartz crystals first grew along cooler sidewalls or against the roof, then were picked up and transferred by magma movements to slightly warmer zones (Wolff *et al.*, 2002).

DISCUSSION

A thermal signature recorded in quartz?

Based on our analysis above, we can state with confidence that the observed compositional variations, commencing within quartz of UBT unit 3, are the result of changing thermal conditions within the Valles magma chamber. Apparent temperatures were increased by at least 35–140°C, with some data suggesting greater increases (Fig. 9; also see Supplementary Data Table 5). Multiple independent lines of evidence provide additional support for a temperature increase at higher stratigraphic levels within the UBT outflow sheets.

Phase equilibria evidence

First, a systematic increase in pre-eruptive temperature and also oxygen fugacity is recorded by oxide–silicate and two-pyroxene geothermometry (Warshaw & Smith, 1988). The Tsankawi Pumice Bed contains titanomagnetite in the presence of fayalite, yielding a minimum crystallization temperature of 697°C and oxygen fugacity of $\log_{10}$ −16·90. UBT unit 3 contains both augite and hypersthene but lacks appreciable fayalite (Table 1), thus the two-pyroxene geothermometer yields a mean temperature of 785°C. The upper ignimbrite unit 5 records a mean two-pyroxene temperature of 805°C, an Fe–Ti oxide temperature of 837°C and $\log f_{O2}$ of −13·01 (Warshaw & Smith, 1988).

Mineralogical and geochemical evidence

As mentioned above, the pressure of the Bandelier magma chamber at eruption was about 200 ± 50 MPa. All previous researchers on the Tshirege ascribed compositional differences to temperature gradients. Caress (1995, 1996) and Phillips (2004, 2007*a*) documented increased compositional variation in rims of alkali feldspars erupted during the waning stages of the UBT ($Or_{<28–44}$), as compared with phenocrysts sampled from the early flow units ($Or_{36–44}$). The occurrence of syenitic crystal clots within UBT units 2 and 3 adds to the range in alkali feldspar Or content. However, considering the rhyolitic component alone, an increase in the range of Or content is still apparent (Caress, 1995). The syenitic clots are thought to be derived from a crystal mush zone tapped during the late stages of the UBT eruption (Caress, 1995). Sanidine is the dominant feldspar within the UBT, but the emergence of

prominent anorthoclase as well as plagioclase armoured by anorthoclase within UBT unit 4 is also documented (Smith & Bailey, 1966; Caress, 1995, 1996; Warren *et al.*, 2007). Concurrent with the increase in compositional variation are a greater number of grains exhibiting disequilibrium (resorption) textures in the late-erupted units. Quartz exhibits a trend similar to the modal phenocryst content, increasing from 5% in the Tsankawi Pumice Bed to around 30% in unit 3, then showing a decrease in the late-erupted units 4 and 5 (Fig. 2). In comparison, the alkali feldspar content shows a steady increase as a proportion of total phenocrysts, from 60% in the Tsankawi Pumice Bed to 85% in unit 5 (Fig. 2) (Smith & Bailey, 1966; Warren *et al.*, 2007). A decrease in the modal phenocryst content, partial resorption of quartz (and feldspar to some extent), and an increase in the alkali feldspar compositional range are together suggestive that the lower part of the chamber was interacting with a hotter magma.

Several of the Cerro del Medio eruptive units are mapped as obsidian flows, with flow unit 4 forming roughly half of the total 5 km^3 volume of the complex (Gardner *et al.*, 2007). All of the flow units have <5% phenocrysts, mostly sanidine. Both hornblende and embayed quartz crystals are rare, as is plagioclase. The elevated Ti concentrations in quartz of the Cerro del Medio lavas suggest that they may have been relatively hot compared with the early UBT (Fig. 8). If the Cerro del Medio lavas are related to the UBT, they represent a significant volume of hotter, crystal-poor rhyolite from the Valles magma chamber.

Our analyses of Ti in glass for several subunits of the UBT show that Ti concentrations increase upsection through the UBT and continue for post-caldera units such as the Redondo Creek Rhyodacite (Supplementary Data Table 2). These data also suggest hotter conditions at later stages of the Bandelier magma chamber eruptions, as Ti is more soluble in the silicic melt at higher temperatures.

Field evidence

Smith & Bailey (1966) showed that the degree of welding within successive ignimbrite units was related to emplacement temperatures. The Tsankawi Pumice Bed and early ignimbrite units grade from unwelded and crystal-poor to partially welded and vapour-phase altered. UBT unit 3t generally exhibits the highest degrees of welding outside the caldera. The late ignimbrite units also show similar horizons of dense welding, especially vitrophyric horizons prominent within intracaldera unit 5u (Goff *et al.*, 2007). Collectively, this upsection increase in the degree of welding cannot be explained by an ignimbrite emplaced at uniformly low temperatures (Smith & Bailey, 1966).

A minor population of fine-grained, hornblende dacite pumices (67–69 wt % SiO_2) is present within the Tsankawi Pumice Bed and interspersed throughout the lower UBT. Importantly, there is no evidence for this pumice type within the immediately underlying tephra units of the Cerro Toledo Formation. Therefore the dacite pumices are suggestive of new magma entering the Bandelier system within a short period prior to eruption. A number of studies have shown that inputs of more mafic magma induce a temperature increase within a chamber containing silicic magma (e.g. Snyder, 2000; Wark *et al.*, 2007; Wiebe *et al.*, 2007; Campbell *et al.*, 2009).

These various lines of evidence support the presence of a pronounced thermal gradient within the Bandelier magma chamber prior to eruption of the UBT (e.g. Hildreth, 1981; Wark *et al.*, 2007). A fundamental question is whether the thermal gradient represents tapping of incrementally deeper and hotter levels of the chamber or the input of hot new magma, or both. We use the quartz zoning patterns to answer this question. First, rims on zoned quartz crystals are invariably high-temperature. Second, core regions are ubiquitously low-temperature and rounded. These two observations are highly suggestive of interaction with hot, new magma entering the chamber. The timing of injection and origin of this magma are discussed in the following sections.

Relative timing of magmatic recharge

A key question is whether the quartz zoning is a reflection of a relatively short or protracted magmatic recharge event or events. We have multiple lines of evidence suggesting that a recharge event occurred relatively soon before eruption of the UBT.

The lack of hornblende dacite pumices within the preceding Cerro Toledo Formation suggests that the parental material was incorporated into the chamber within a geologically short period following termination of CTF volcanism, just prior to eruption of the UBT (e.g. Self *et al.*, 1986; Stimac *et al.*, 1996; Warren *et al.*, 2007). Petrographic analysis of the hornblende dacite pumices reveals both cogenetic phenocrysts and a component of reacted xenocrysts of alkali feldspar and resorbed quartz derived from the UBT, which suggests that this more primitive magma interacted with the rhyolitic magma (Stimac *et al.*, 1996). In addition, the abundance of plagioclase and hornblende phenocrysts within the Tsankawi Pumice Bed and UBT unit 1g indicates that these crystals are derived from mixing of two distinct magmas prior to and during the early phases of eruption (Warren *et al.*, 2007). Within some UBT rhyolitic pumices, it is common to find a trace component of hornblende, plagioclase and pyroxene crystals with chemistry similar to that of the hornblende dacite pumices (Stimac *et al.*, 1996). Some of these minerals are themselves rimmed by a fine-grained matrix, suggesting that they were derived from disaggregation of the hornblende dacite pumice (Stimac *et al.*, 1996).

The outer high-intensity CL zones of quartz crystals from UBT units 3–5 record temperatures ~35–140°C hotter than at the start of the caldera-forming eruption.

Concurrent with the occurrence of zoned quartz crystals, the boundaries between core and rim are often sharply defined (Fig. 7) with Type 1 reverse zoning dominant (Fig. 6). The resulting increase in the titanium concentration occurs over a distance <40 μm for most zoned crystals (Fig. 7i). The ubiquitous rounding of the core regions of a large proportion of the quartz crystals suggests an event that affected a significant proportion of the Bandelier magma chamber, leading to widespread crystal resorption. This evidence demonstrates that the temperature of the Bandelier chamber was raised (~35–140°C) to promote partial dissolution of quartz, with subsequent growth of high-temperature outer rims on quartz from the later-erupted ignimbrite units.

We can use the known diffusivity of titanium within quartz at a given temperature to assess the relative growth rates of these outer zones. The diffusivity of Ti (D_{Ti}) is given by the Arrhenius relation

$$D_n = 7 \times 10^{-8} \exp\left(\frac{-273 \pm 12 \text{ kJ mol}^{-1}}{RT}\right) \text{m}^2 \text{ s}^{-1} \quad (4)$$

where R is the universal gas constant and T is the temperature in Kelvin. From this equation, we can determine the time elapsed since the onset of diffusion (D) over a distance (d), given by the relation

$$t = \frac{d^2}{4D}. \quad (5)$$

In this case the thickness of the zone boundary is representative of d. For example, the calculated average boundary thickness within quartz from UBT unit 3 is 28·5 μm, based on image analysis of six crystals. Furthermore, zoned quartz crystals from the porphyritic Deer Canyon Rhyolite show similar zone boundary widths (e.g. Fig. 7a). Based on the temperature estimates of Warshaw & Smith (1988), a mean temperature of 1058 K (785°C) is used for unit 3 (Supplementary Data Table 2). Using a range of Ti diffusion rates and the calculated zone boundary widths, the time for the observed diffusion within the quartz crystals used for this study ranges from 1080 to 7340 years. This is similar to the ~10^4 year duration of a recharge event occurring before eruption of the Otowi member of the Bandelier Tuff, calculated using Sr diffusion in sanidine (Hervig & Dunbar, 1992). Thus, the temperature increase required for subsequent crystallization of high-Ti rims on quartz may have occurred a few thousand years or less prior to eruption.

Nature of the injected magma

Based on field exposures, the dacite pumices make up <1 vol. % of the UBT (Smith, 1979; Balsley, 1988; Caress, 1995; Stimac *et al.*, 1996), hence <4 km^3 of this more mafic magma was erupted, presumably having resided at the roof region of the reservoir before eruption, as it is found primarily within the Tsankawi Pumice Bed. The hornblende dacite magma may have ascended rapidly through the Bandelier chamber owing to thermal and density contrasts (Blake, 1981; Blake *et al.*, 1992). Smith (1979) envisaged that the Bandelier chamber (which contained both the Otowi and Tshirege, or Upper Bandelier Tuff magmas) was underlain by a substantial volume of melt, rhyodacitic in composition, which was in turn underlain by a deeper basaltic zone. With regard to the hornblende dacite pumices, several possibilities exist as to their ultimate origin. First, they may simply be a sample of a pre-existing dacite source that underwent little or no interaction with the UBT, although mineral exchange probably occurred (Gardner *et al.*, 1986; Stimac *et al.*, 1996). Second, the hornblende dacite pumice could be a hybrid composition resulting from intrusion and mingling of a more mafic magma into a rhyolitic chamber. There may be some evidence for a basaltic source in the Mg-rich pyroxenes and the most calcic zones of some plagioclase crystals. However, textural and mineralogical evidence suggests that the hornblende dacite magma existed as a discrete layer within the Bandelier chamber shortly before eruption (Stimac *et al.*, 1996). There was a degree of mixing and mingling between the two magmas, and vesiculation by partial quenching of the hotter dacite probably caused a small volume of this material to become buoyant and rise into the roof regions of the chamber, where it was erupted synchronously with the Tsankawi Pumice Bed (Stimac *et al.*, 1996).

Several researchers have remarked upon the close geochemical similarity of the hornblende dacite pumices to the Cerro Rubio dacite, erupted during late Tschicoma volcanism at 3·59–4·21 Ma (Gardner *et al.*, 1986; Heiken *et al.*, 1986; Goff *et al.*, 2011). Based on major elements, there is close geochemical agreement between the two magma compositions (see Supplementary Data Table 4). However, the large variation of trace elements precludes any simple derivation and warrants further investigation.

The close spatial relationship between the Bandelier magma chamber and Cerro Rubio raises the possibility of a volume of coexisting Tschicoma dacite melt being injected into the Bandelier system and forming the hornblende dacite pumices. It is clear that the dacite pumices do not share any clear geochemical relationship to the UBT, as there is poor agreement between the trace element geochemistry of the hornblende dacite and the UBT (Fig. 10).

It is possible that magma recharge was not limited to periods before eruption, and may have continued throughout the period examined in this study. Warren *et al.* (1997, 2007) showed that anorthoclase-rich samples of UBT unit 4 have unusual geochemistry. Notable spikes in Ti, Sr, Ba, and Zr within this unit depart from the overall UBT trends (see Warren *et al.*, 2007, table 1). An injection of more primitive magma may have created this geochemical

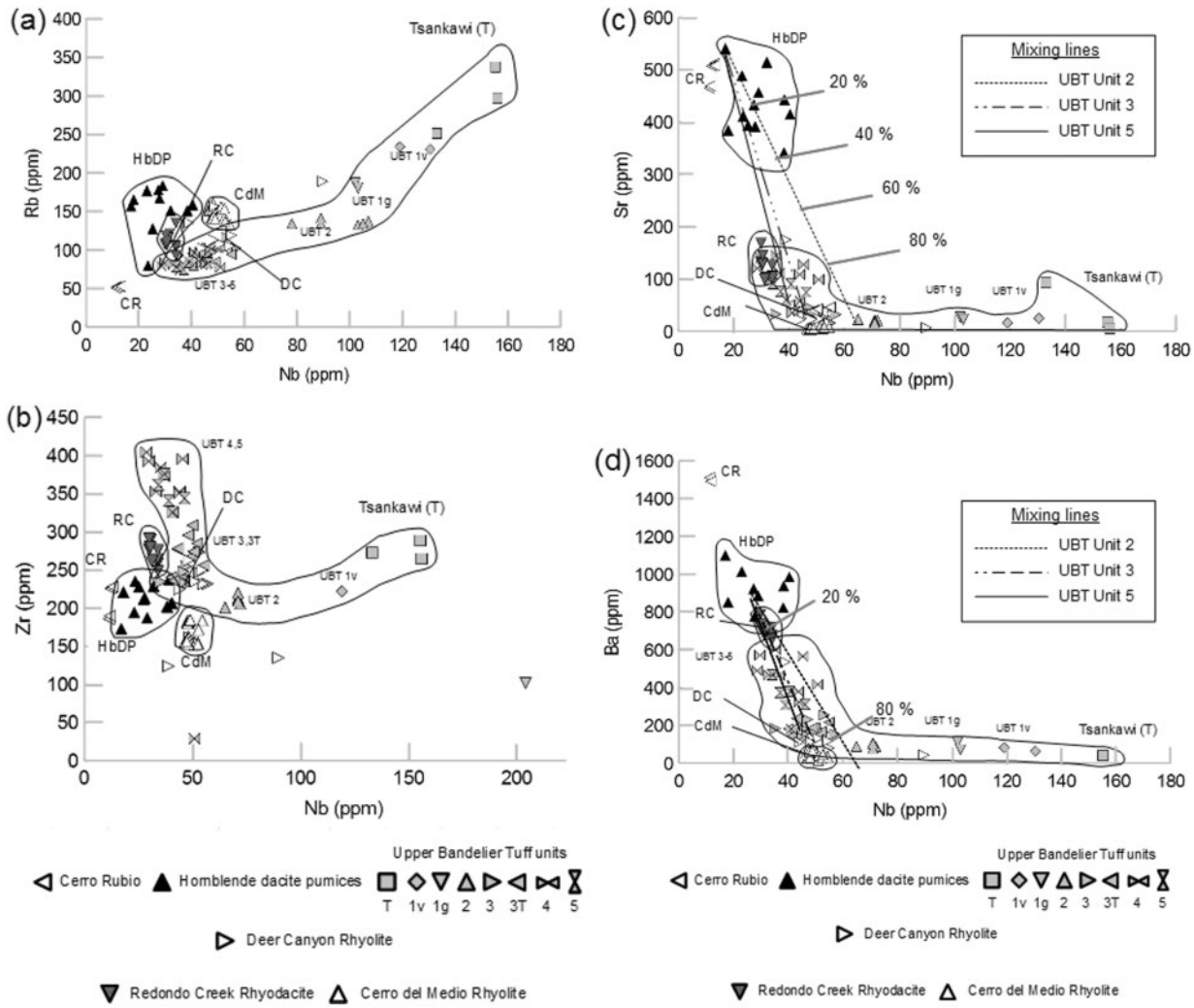

Fig. 10. Trace element variation diagrams showing the relationships among the Upper Bandelier Tuff (UBT), Deer Canyon Rhyolite (DC), Redondo Creek Rhyodacite (RC), Cerro del Medio Rhyolite (CdM), hornblende dacite pumices (HbDP) and Cerro Rubio dacite (CR). The Bandelier geochemical trend progresses from the early erupted Tsankawi pumice bed (T) to the late upper ignimbrite units (UBT 4 and 5). Each subunit is represented by a separate symbol, indicated on the legend. The reader is referred to Supplementary Data Table 4 for a comprehensive geochemical database of units applicable to this study. (c) and (d) show mixing lines between the most primitive samples of hornblende dacite pumice and the most evolved samples from UBT units 2, 3 and 5, respectively. The percentage incorporation of UBT rhyolite is shown for reference.

trend. Thus, the prominent anorthoclase, as well as plagioclase armoured by anorthoclase within UBT unit 4, could be the product of mixing between rhyolite and a more primitive magma that was distinct from the hornblende dacite injected before the UBT eruption (Warren *et al.*, 2007).

Pre-eruptive thermal regime of the UBT

The abrupt appearance and occurrence of zoned quartz crystals within the mid-to-late ignimbrite units is intriguing. Extensive mapping of the UBT outflow sheets has identified that units 1g, 1v and 2 make up ~70% of the entire volume of the 400 km^3 ignimbrite sequence. Our complementary titanium-in-quartz measurements hence indicate that a large volume of the ignimbrite was erupted from a portion of the Bandelier chamber that had been at a relatively uniform temperature (Supplementary Data Table 5). However, given that a significant proportion of these quartz grains show evidence of partial resorption, these temperatures are reflective of conditions prevalent before the heating event or events commenced. The occurrence of zoned quartz crystals within units 3–5 suggests that the deeper portion of the chamber was periodically subject to thermal disequilibrium, and the high-temperature outer rims are evidence of growth from a hotter magma.

Based on the geochemistry of alkali feldspar phenocrysts, the model of Caress (1995, 1996) proposes that the Bandelier magma chamber was composed of two main horizons. The upper portion of the chamber contained the magma that erupted as the Tsankawi Pumice Bed and ignimbrite units 1 and 2 of the UBT, representing collectively over 70% of the erupted volume. Within the upper portion of the magma chamber, unzoned sanidine with $Or_{36–44}$ was the dominant alkali feldspar. The lower level residuum of the chamber is represented by the late-erupted units 3–5, and the increased geochemical variation in alkali feldspar chemistry ($Or_{<28}$–Or_{44}) is a reflection of a more dynamic, convecting region.

The role of pressure

The original *TitaniQ* geothermometer of Wark & Watson (2006) has been recently modified by Thomas *et al.* (2010) and Huang & Audétat (2012) to account for pressure effects on the solubility of titanium in quartz. The original experiments utilized a working pressure of 1000 MPa; Thomas *et al.* (2010) extended this to a range of 500–2000 MPa, whereas Huang & Audétat (2012) used a range of 1000–10 000 MPa. Both studies show that a systematic decrease in Ti concentration in quartz occurs with increasing pressure, although the two models yield different results owing to differences in crystal growth rates and Ti solubilities.

One way of applying this revised geobarometer is to the high-Ti rims on quartz from UBT units 3–5, which could be representative of growth within a melt residing at lower pressures than those prevalent during low-Ti core growth. We calculate pressures in two ways: (1) by using the independent temperature estimates of Warshaw & Smith (1988); (2) by assuming a constant temperature of 700°C. We take a similar approach to that we used for temperature by calculating pressure differences between the early erupted units (Tsankawi Pumice Bed and UBT units 1g and 2) and late-erupted units (units 3–5). In general, our calculations reveal that the early units have higher pressures compared with the later units. We also use the same four datasets of TiO_2 activity as were used for temperature. All calculations are shown in Supplementary Data Table 5.

Using the Thomas *et al.* (2010) algorithm, pressures range from 690 to 1360 MPa using the Warshaw & Smith (1988) temperatures. When a constant temperature of 700°C is applied, pressures range from 650 to 1190 MPa. In other words, the calculated pressures indicate very deep crustal environments for all samples including early erupted and late-erupted. This is clearly a problem, as a shallow crustal magma reservoir is indicated at Valles by (1) the seismic tomographic studies, (2) the water contents of ~4–6 wt % in melt inclusions, and (3) a large caldera depression.

Results using the Huang & Audétat (2012) algorithm are shown in Fig. 11. Using the Warshaw & Smith (1988) temperatures (Fig. 11a), pressure differences show two groupings. For TiO_2 activities of 0·5 and as calculated from Hayden & Watson (2007), pressure differences are 100–300 MPa with absolute pressures of 234–671 MPa. For TiO_2 activities calculated from *TitaniQ* and MELTS TiO_2 activities, the pressure differences are significantly smaller with absolute pressures of 116–268 MPa. This second set of results is very interesting, as it essentially matches the pressures calculated independently by other workers.

Assuming a constant temperature of 700°C, the results are similar (Fig. 11b). For TiO_2 activities of 0·5 and as calculated from Hayden & Watson (2007), pressure differences are between 200 and 400 MPa, and absolute pressures are 58–563 MPa. For TiO_2 activities calculated from *TitaniQ* and MELTS TiO_2 activities, pressure differences are less than 150 MPa and absolute pressures 38–278 MPa.

Given the uncertainties with the current models and with the estimates of titanium activity and temperatures, it is difficult for us to be definitive about the role of pressure at Valles. There are two possibilities. The first is that pressure changes are not significant. This scenario is suggested by the *TitaniQ* and MELTS data shown in Fig. 11a, where the pressure differences are close to zero and the absolute pressures correspond to those calculated by independent means. Second, if pressure is playing an important role here, it can be envisaged in two different ways. During a caldera-forming eruption, the pressure regime of the magma reservoir changes rapidly from a state of overpressure at the beginning of the eruption to an underpressured state at the end of the eruption (Martí *et al.*, 2000). In such a case, pressure changes of the order of 100 MPa appear reasonable, whereas variations of 200–400 MPa may be too high (Martí *et al.*, 2000; Stix & Kobayashi, 2008). Alternatively, quartz crystals may have ascended from a deeper region to a shallow crustal level, as suggested by Thomas *et al.* (2010). The rate at which this transfer occurred was presumably rapid, to account for the sharp nature of zone boundaries between the core and rim.

In summary, based on the available evidence for a shallow magmatic system beneath Valles Caldera, we prefer a simple model in which a shallow reservoir is periodically replenished by more primitive magma from below. We acknowledge the possibility that the quartz grains that we have studied may have experienced different pressure regimes, either through a cycle of underpressure during the caldera-forming eruption or by transport from deeper crustal levels. This is clearly an area of active research that requires further work to elucidate these interesting and complex issues.

Resurgence: origin of the post-UBT magmas

Deer Canyon Rhyolite

Following caldera collapse, the Bandelier magma chamber was in a state of disequilibrium. Our Ti-in-quartz results

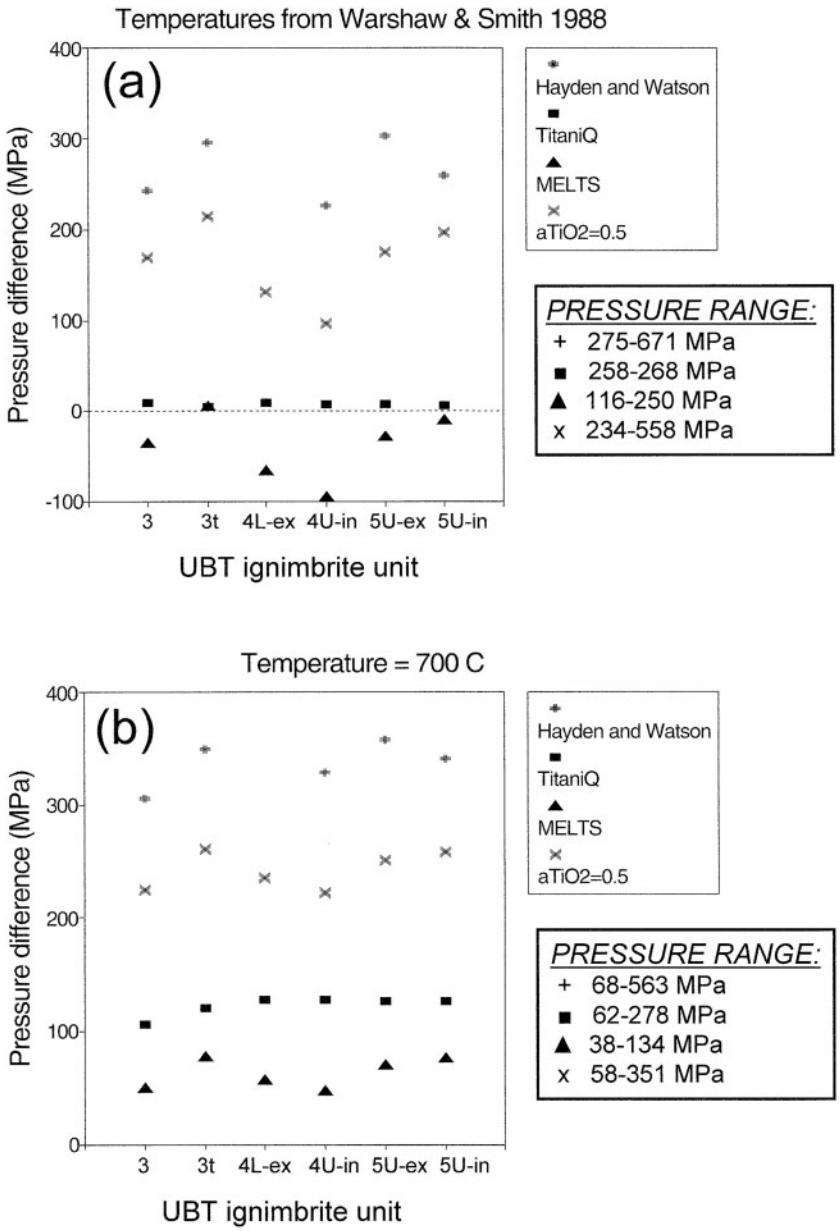

Fig. 11. Calculated pressure differences between the low-titanium cores and high-titanium rims of UBT units 3 to 5U. The pressure differences plotted are relative to the average calculated pressure of the combined Tsankawi pumice, UBT 1g and UBT 2, which represent 70% of the erupted volume of the UBT. (a) Pressure differences using temperatures from Warshaw & Smith (1988). (b) Pressure differences using a constant temperature of 700°C. Pressures were calculated using the *TitaniQ* expression of Huang & Audétat (2012) with four methods of estimating TiO_2 activities in the melt. Absolute pressure ranges are also indicated for each TiO_2 activity used. (See text for details.)

from the Deer Canyon Rhyolite suggest that these lavas probably originated from distinct regions of the chamber following collapse. There is marked contrast in the zoning patterns of both quartz and feldspar between lavas erupted on the western resurgent dome (sample 13, porphyritic with zoned quartz and feldspar) and those from central dome locations (sample 15, less abundant, smaller, unzoned quartz and feldspar). In fact, the Deer Canyon Rhyolite occurs as a fine-grained, crystal-poor lava on the eastern resurgent dome, contrasting with its extremely porphyritic nature within western regions (Goff *et al.*, 2007, 2011). Gibler (2004) also shows that the easternmost flow lobes are relatively crystal-poor (2–6% phenocrysts), containing little or no quartz. Thus, even though we rely on two samples of Deer Canyon Rhyolite for the purpose of this study, a trend toward crystal-poor eastern lavas has also

been documented by other workers. Therefore, we believe our two samples are representative of the range in crystal content of this unit. Furthermore, comprehensive dating and fieldwork (Phillips, 2004; Goff *et al.*, 2007, 2011; Phillips *et al.*, 2007*b*) have shown that all Deer Canyon lava flows and tuffs were erupted within the period 1·229–1·283 Ma.

A pertinent question is whether the Deer Canyon eruptions sampled two distinct reservoirs, as suggested by Gibler (2004) and Goff *et al.* (2007), or if the heterogeneity is the result of new magma intruding locally into a single chamber. A two-reservoir hypothesis is difficult to reconcile with the similar mineralogy and geochemistry of the Deer Canyon Rhyolite and the later-erupted UBT (Fig. 10) (Spell *et al.*, 1993; Phillips, 2004). The Deer Canyon lavas appear to be depleted in Ba, Sr and Zr relative to the late-erupted UBT units 4 and 5, although most samples have undergone some degree of alteration (Fig. 10; Phillips, 2004; Goff *et al.*, 2007). The titanium concentrations of (1) cores of zoned quartz from the porphyritic rhyolite and (2) unzoned quartz from the crystal-poor rhyolite are similar to the core concentrations of UBT quartz (Fig. 8). This suggests that the quartz crystals of the Deer Canyon Rhyolite and the UBT were subjected to similar thermal conditions.

To generate the heterogeneity in quartz zoning and crystal content, a possible mechanism may involve intrusion of new magma into a residual crystal mush, of a composition similar to the last erupted unit of the UBT. Intrusion may have been localized, leading to extensive quartz resorption in certain areas, hence producing the crystal-poor or aphyric nature of the central and eastern lavas.

Detailed intra-caldera drilling has revealed that caldera collapse was both piecemeal and trapdoor in nature, with maximum subsidence to the east where the intra-caldera UBT is thickest (Goff, 1983; Heiken *et al.*, 1986; Self *et al.*, 1986). The crystal-poor nature of the Deer Canyon lavas in the east may therefore be related to the increased subsidence of the caldera roof blocks, which probably sank into the crystal mush, inducing convective mixing. The occurrence of synneusis textures in the eastern lavas (sample 15) suggests a low-energy environment of sufficient fluidity to permit crystal entrainment (Vance, 1969; Vernon, 2004). A plausible process for development of this texture is expulsion of crystal-poor melt from a mush zone, which had previously been heated, as suggested by the occurrence of widespread resorption textures (Gibler, 2004). Under application of downward pressure, it is feasible to expel significant volumes of crystal-poor rhyolite and facilitate crystal attachment (synneusis texture) from a mush zone of rhyodacitic composition (Bachmann & Bergantz, 2004; Kennedy *et al.*, 2008; Girard & Stix, 2009). This process may have been important during formation of the crystal-poor Deer Canyon Rhyolite.

The porphyritic Deer Canyon Rhyolite erupted onto the western resurgent dome may be derived from more crystal-rich horizons in the residual Bandelier magma chamber. Conditions favoured crystal growth, and temperatures were probably similar to those prevailing at the end of the UBT eruption, as there is close agreement in the values and the range of Ti concentrations for rims of quartz from UBT units 3–5 and the porphyritic Deer Canyon Rhyolite (Fig. 8).

In summary, the mineralogical diversity of the Deer Canyon Rhyolite may be a product of several processes: (1) interaction with hot new primitive magma; (2) variable caldera collapse; and/or (3) expulsion of small-volume magma batches from a crystal mush.

Redondo Creek Rhyodacite

The processes driving resurgence were first discussed in the seminal work by Smith & Bailey (1968), one scenario involving new input of magma at depth. The occurrence of the hornblende dacite pumices within the initial eruptive products of the UBT could indicate that resurgence may be a response to injection of intermediate composition magma. The mineralogy exhibited by the Redondo Creek Rhyodacite is unusual and distinct from that of the UBT and the Deer Canyon Rhyolite. The lack of quartz, as well as the presence of anti-rapikivi feldspars (sieve-textured plagioclase cores with sanidine rims) and abundant biotite and Fe–Ti oxides, suggests a complex relationship.

Smith & Bailey (1968) hypothesized that the Redondo Creek Rhyodacite represents the product of chamber overturn following withdrawal and eruption of the UBT. This unit has a trace element chemistry that is transitional between that of the UBT and the hornblende dacite pumice (Fig. 10). Based on this evidence, a key question is whether the Redondo Creek Rhyodacite represents mixing of two distinct sources or a new input of relatively primitive magma. The first scenario is supported by our geochemical data, where the Redondo Creek Rhyodacite could be derived from mixing of residual UBT and renewed input of Tschicoma-like hornblende dacite. However, several lines of reasoning complicate this process. First, the composition of the UBT parental magma is unclear, as the scatter of incompatible elements within the late-erupted UBT units suggests that these also may represent a partially hybridized magma (Fig. 10). Stimac *et al.* (1996) suggests that the hornblende dacite pumice is the product of mixing between a more mafic member (possibly andesitic) and rhyolite of composition similar to UBT units 2 and 3, which exhibit less geochemical heterogeneity than do later ignimbrite units. To generate a composition similar to the Redondo Creek Rhyodacite, a simple mixing model between the hornblende dacite pumice and rhyolite of UBT units 2 and 3 generally works for Ba but not for Sr. This discrepancy is also indicated by Sr vs Nb and Ba vs Nb

plots (Fig. 10c and d). In the case of Sr, the model requires 80% incorporation of UBT rhyolite to derive the Redondo Creek Rhyodacite. With Ba, however, only 40% rhyolite is required. The UBT endmember may in fact be a more primitive composition, similar to Deer Canyon Rhyolite, which would improve some but not all linear mixing trends. Thus, simple mixing of hornblende dacite and UBT rhyolite may not be the controlling factor in the formation of the Redondo Creek Rhyodacite.

An alternative scenario is that the Redondo Creek Rhyodacite itself represents a distinct magma, as suggested by Gibler (2004). Indeed, the Redondo Creek Rhyodacite exhibits a tight grouping in terms of geochemistry, as does the Cerro del Medio Rhyolite (Fig. 10). The marked difference in mineralogy between the Redondo Creek Rhyodacite and both the Deer Canyon Rhyolite and the UBT could also be suggestive of a distinctive magma.

Cerro del Medio Rhyolite

It appears unlikely that the Cerro del Medio Rhyolite is sourced from the Bandelier chamber following eruption of the UBT and resurgence-related units, based on geochemical and isotopic data (Fig. 10; Spell *et al.*, 1993, and references therein). There are several alternatives. The elevated titanium concentrations in unzoned quartz crystals of the Cerro del Medio complex indicates that crystallization temperatures may have been hotter than those prevailing before eruption of the UBT. Gardner *et al.* (2007) estimated the cumulative volume of Cerro del Medio to be $<5\ km^3$; thus, the underlying magma chamber (one distinct from the Bandelier) may have been relatively small, perhaps of the order of $10–15\ km^3$ (Spell *et al.*, 1993). Based on our CL imaging and Ti-in-quartz data, this chamber was possibly isothermal (>800°C). The unzoned but hot nature of the quartz crystals may be indicative of a relatively short residence time in a hot magma, which did not permit the development of zoning in quartz. Alternatively, the Cerro del Medio lavas may be products of remelting of a crystal mush at depth (Gibler, 2004). This mush zone may represent residual UBT material, or perhaps a hybrid derived from mixing of new magmas during resurgence. The latter scenario could explain the isotopic trends identified by Spell *et al.* (1993) who suggested that the post-collapse rhyolites are the products of intermittent eruptions from an upper crustal magma chamber thermally sustained by basaltic injections. Evidence is so far unsupportive of a direct relationship to the UBT, although many studies have illustrated that reactivation of a crystal mush is an important mechanism in post-caldera volcanism (e.g. Hildreth, 2004; Hildreth & Wilson, 2007; Bachmann & Bergantz, 2008; Girard & Stix, 2009, 2010).

CONCLUSIONS

Based on the results of this work and a synthesis of other studies, we propose the following four-stage model for the thermal evolution of the Bandelier magmatic system from 1·256 Ma to ~1·11 Ma (Fig. 12). This ~150 kyr period encompasses eruption of the Tshirege (Upper) Member of the Bandelier Tuff and collapse of the Valles Caldera, resurgence of the caldera and associated volcanism, and eruption of the initial ring fracture rhyolite into the caldera moat following termination of resurgence. Most significantly, we have documented a magmatic recharge event prior to eruption of the Upper Bandelier Tuff (UBT). Furthermore, recharge probably occurred throughout the UBT eruption, as well as during resurgence of the caldera, either as a continual process or as a series of discrete events. This is manifested by the compositional heterogeneity of late UBT units as well as lavas erupted during resurgence, in particular the Redondo Creek Rhyodacite.

Although the ultimate source of the recharging magma is debatable, this hotter, more primitive magma appears to be dacitic in composition and underwent a limited amount of mixing and mingling with the rhyolite magma of the UBT, forming a discrete layer in the chamber. Recharge of the Bandelier system commenced <10 kyr before eruption. The heat provided by this magma led to widespread crystal resorption. With regard to quartz, this resorption event left rounded cores of low titanium concentration. The intruding hornblende dacite magma vesiculated and was partially quenched, forming a magmatic foam that subsequently rose into the roof region of the Bandelier chamber. This process probably induced overpressure in the chamber and triggered the UBT eruption (Stimac *et al.*, 1996).

The cataclysmic eruption commenced with a plinian eruption, depositing the Tsankawi Pumice Bed along with the bulk of the hornblende dacite pumice. Similar to the Tsankawi, the subsequent ignimbrite units lg, lv and 2 of the UBT contain predominantly rounded and unzoned quartz crystals of low titanium concentration. These units form ~70% of the total $400\ km^3$ erupted volume, demonstrating that the UBT magma chamber was largely static and stable prior to its heating from intrusion of the recharging magma.

The lower portion of the chamber, represented by the late-erupted UBT ignimbrite units 3–5, was affected by continual or repeated intrusion of hotter, more primitive magma. High-temperature rims on quartz indicate that these crystals were subject to temperatures at least ~35–140°C hotter than those recorded by core Ti concentrations. In fact, temperatures must have been raised significantly more than this to induce resorption of the core regions before quartz crystallization recommenced, forming the high-temperature rims. Convection induced by

hot recharging magma and caldera collapse led to development of multiple growth zones on quartz and compositional heterogeneity in alkali feldspar within the late-erupted UBT units.

Following the UBT eruptions, the chamber was in a state of temperature and pressure disequilibrium. New magma may have been intruded at this stage into a residual crystal mush of a composition similar to the late-erupted UBT, as

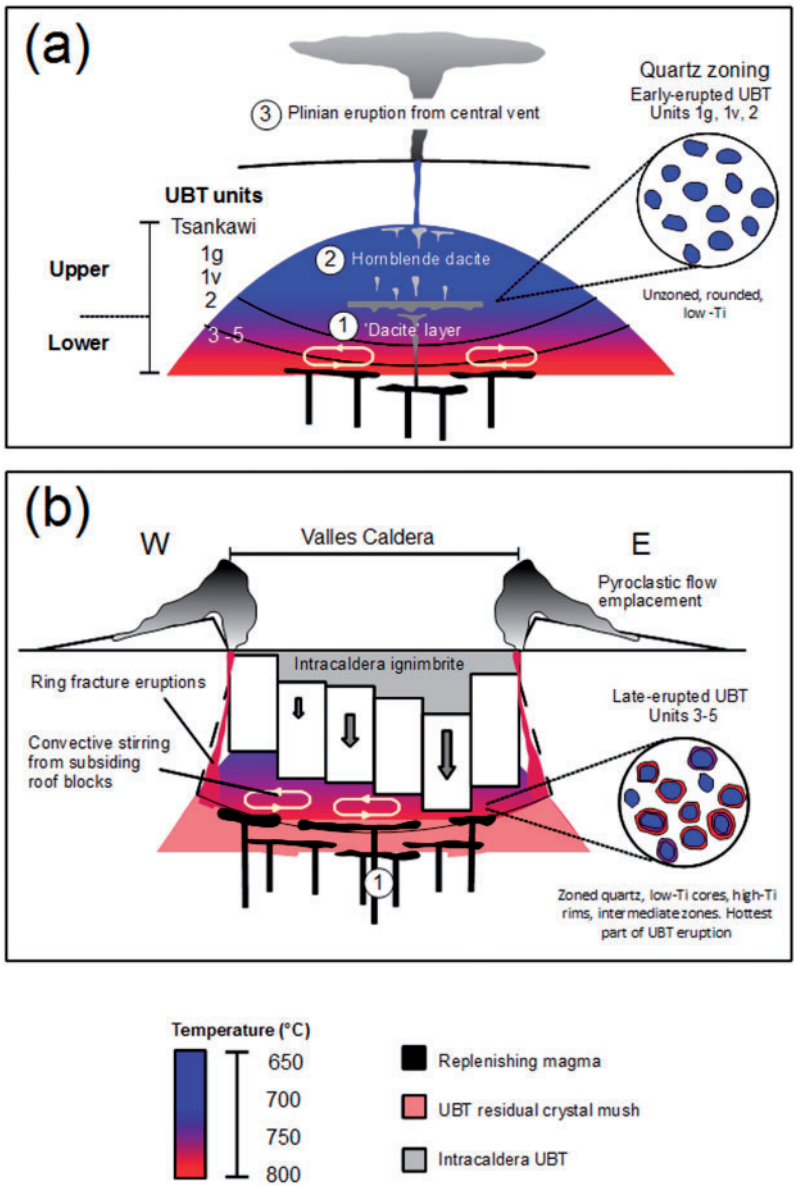

Fig. 12. Four-stage thermal evolution model of the Bandelier magmatic system during collapse and resurgence of the Valles Caldera. (a) Magmatic recharge commences <10 kyr prior to eruption of the Upper Bandelier Tuff, initially heating the entire chamber and causing widespread crystal resorption. Following this, the Bandelier chamber is composed of a voluminous upper layer and a lower convecting layer experiencing thermal disruption. (1) Intrusion of relatively mafic magma into the Bandelier chamber forms a discrete horizon of hybrid composition, which undergoes a limited amount of mingling and mixing with the surrounding rhyolitic magma of composition similar to units 1 and 2 of the UBT. (2) Partial quenching of the hybrid magma forms the hornblende dacite magma. Vesiculation induced by this process provides buoyancy to the hornblende dacite, which rises into the roof region of the Bandelier chamber, residing with rhyolitic magma of a composition similar to that of the Tsankawi Pumice Bed (Stimac *et al.*, 1996). (3) The release of volatiles through partial quenching of the hornblende dacite leads to overpressure in the chamber and eruption of the UBT initially from a central vent. (b) Caldera collapse and formation of the Valles Caldera along ring faults. Maximum subsidence of roof blocks is to the east, forming a piecemeal, trapdoor-style collapse and thick deposits of intra-caldera ignimbrite. The late-erupted UBT units 3–5 contain quartz crystals with complex zoning and high-temperature rims. These are the product of higher temperatures and convective mixing induced by the subsiding roof blocks. (1) New magma may have been drawn into the chamber during caldera collapse, creating geochemical heterogeneity in late-erupted units.

(continued)

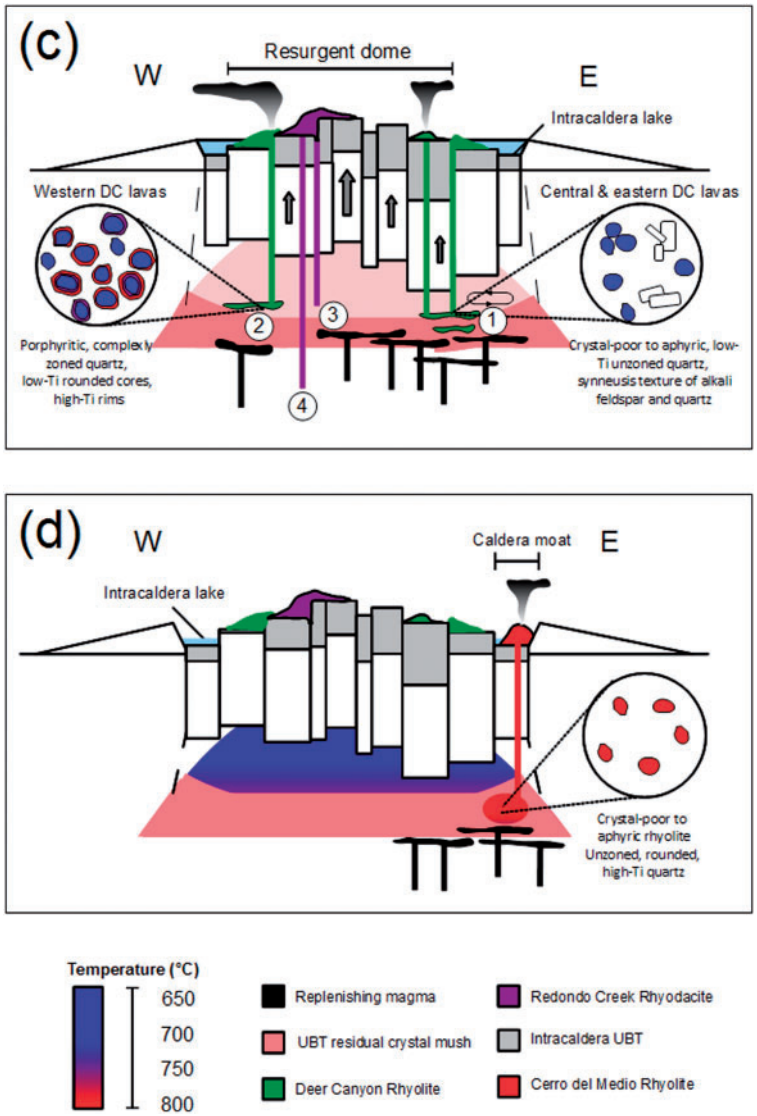

Fig. 12. (c) Resurgence of the Valles Caldera. Maximum resurgence of ~1000 m is confined to the central area of the caldera. The thermal heterogeneity exhibited by the Deer Canyon Rhyolite is a product of differing degrees of interaction between a replenishing magma and a residual UBT crystal mush. (1) The crystal-poor to aphyric lavas on the eastern resurgent dome may have been derived from a partially melted crystal mush, whereas (2) the porphyritic lavas in the west were sourced from a cooler part of the chamber. The Redondo Creek Rhyodacite may represent a hybrid mix of replenishing magma and residual UBT (3), or a distinct magma in itself (4). A temperature gradient for the Bandelier magma chamber is indeterminable during caldera resurgence, so we have indicated a lighter colour for the magma simply to distinguish it from the crystal mush zone. (d) Ring fracture volcanism following termination of resurgence. The foci of volcanism in the Valles Caldera shifted to the easternmost parts of the caldera where the Cerro del Medio Rhyolite complex was erupted. The sparsely porphyritic to aphyric nature of these lavas suggests that they were sourced from hot, small-volume rhyolite batches expelled from the crystal mush.

manifested by the Deer Canyon Rhyolite, which shows thermal heterogeneity, based on Ti-in-quartz data. Increased subsidence of the caldera floor to the east may have led to greater interaction of the intruding magma with the crystal mush, leading to partial melting of the mush and eruption of crystal-poor Deer Canyon Rhyolite onto the central and eastern resurgent dome. Conversely, the western porphyritic lavas exhibit complexly zoned quartz crystals, which may have been derived from a cooler or more crystal-rich portion of the mush that underwent less interaction with replenishing magma.

We theorize that intrusion of the Redondo Creek Rhyodacite magma into the base of the residual chamber caused resurgence. Independent temperature estimates show that this magma was hot (810°C) and may have partially melted the residual UBT crystal mush.

The Cerro del Medio Rhyolite quartz crystals are unzoned and exhibit elevated titanium concentrations

(>40 ppm) compared with cores of UBT and Deer Canyon Rhyolite quartz. This contrast suggests elevated temperatures and isothermal conditions. The Cerro del Medio complex shows little geochemical and isotopic affinity to the UBT and may have been erupted as a series of small-volume, crystal-poor to aphyric rhyolite batches from the UBT crystal mush.

ACKNOWLEDGEMENTS

The authors are grateful for the critical and thought-provoking comments from V. Smith, C. Annen, J. Thomas, and an anonymous reviewer on earlier versions of this paper. J.W. would like to thank Bob Martin for useful comments on the paper's content, and Don Marshall from Relion Industries for valuable orientation and troubleshooting advice with the CL instrument. George Panagiotidis carefully prepared all grain mounts and thin sections. Lang Shi provided assistance with the electron microprobe, and Glenna Keating performed the XRF analyses. Input from members of the McGill Volcanology Research Group is gratefully acknowledged. We thank the Valles Caldera National Preserve for access rights.

FUNDING

Funds for this work were provided to J.S. from the Natural Sciences and Engineering Research Council of Canada, and from Le Fonds Québecois de la Recherche sur la Nature et les Technologies.

SUPPLEMENTARY DATA

Supplementary data for this paper are available at *Journal of Petrology* online.

REFERENCES

Acocella, V. (2010). Evaluating fracture patterns within a resurgent caldera: Campi Flegrei, Italy. *Bulletin of Volcanology* **72**, 623–638.

Aldrich, M. J., Jr, Chapin, C. E. & Laughlin, A. W. (1986). Stress history and tectonic development of the Rio Grande rift, New Mexico. *Journal of Geophysical Research* **91**, 6199–6211.

Annen, C. (2009). From plutons to magma chambers: Thermal constraints on the accumulation of eruptible silicic magma in the upper crust. *Earth and Planetary Science Letters* **284**, 409–416.

Aprea, M., Hildebrande, S., Fehler, M., Steck, L., Baldreidge, W., Roberts, P., Thurber, C. & Lutter, W. (2002). Three-dimensional Kirchhoff migration: Imaging of the Jemez volcanic field using teleseismic data. *Journal of Geophysical Research* **107**, 2247–2262.

Asimow, P. D. & Ghiorso, M. S. (1998). Algorithmic modifications extending MELTS to calculate subsolidus phase relations. *American Mineralogist* **83**, 1127–1131.

Bachmann, O. & Bergantz, G. W. (2004). On the origin of crystal-poor rhyolites: extracted from batholithic crystal mushes. *Journal of Petrology* **45**, 1565–1582.

Bachmann, O. & Bergantz, G. W. (2008). Deciphering magma chamber dynamics from styles of compositional zoning in large silicic ash flow sheets. In: Putirka, K. D. & Tepley, F. J., III (eds) *Minerals, Inclusions and Volcanic Processes. Mineralogical Society of America and Geochemical Society, Reviews in Mineralogy and Geochemistry* **69**, 651–674.

Bailey, R. A., Smith, R. L. & Ross, C. S. (1969). Stratigraphic nomenclature of volcanic rocks in the Jemez Mountains, New Mexico. *US Geological Survey Bulletin* **1274-P**, 1–19.

Balsley, S. D. (1988). The petrology and geochemistry of the Tshirege Member of the Bandelier Tuff, Jemez Mountains Volcanic Field, New Mexico, U.S.A, MSc thesis, University of Texas at Arlington, 188 pp.

Blake, S. (1981). Eruptions from zoned magma chambers. *Journal of the Geological Society, London* **138**, 281–287.

Blake, S., Wilson, C. J. N., Smith, I. E. N. & Walker, G. P. L. (1992). Petrology and dynamics of the Waimihia mixed magma eruption, Taupo Volcano, New Zealand. *Journal of the Geological Society, London* **149**, 193–207.

Broxton, D. E. & Rogers, M. A. (2007). Comparison of two systems of nomenclature for the Tshirege Member, Bandelier Tuff, Central Pajarito Plateau, New Mexico. In: Kues, B. S., Kelley, S. A. & Lueth, V. W. (eds) *Geology of the Jemez Region II. New Mexico Geological Society 58th Annual Field Conference Guidebook*. Socorro: New Mexico Geological Society. pp. 37–39.

Broxton, D. E., Heiken, G. H., Chipera, S. J. & Byers, F. M., Jr (1995*a*). Stratigraphy, petrography and mineralogy of Bandelier Tuff and Cerro Toledo deposits. In: Broxton, D. E. & Eller, P. G. (eds) *Earth Science Investigations for Environmental Restoration—Los Alamos National Laboratory Technical Area 21. LANL Report LA-12934-MS*, pp. 33–63.

Broxton, D. E., Vaniman, D., Byers, F. M., Jr, Chipera, S. J., Kluk, E. C. & Warren, R. G. (1995*b*). Stratigraphy, mineralogy and chemistry of bedrock tuffs at Pajarito Mesa. In: Broxton, D. E. & Eller, P. G. (eds) *Geological site characterization for the proposed mixed waste disposal facility, Los Alamos National Laboratory. LANL Report LA-13089-MS*, pp. 5–30.

Campbell, M. E., Hanson, J. B., Minarik, W. G. & Stix, J. (2009). Thermal history of the Bandelier magmatic system: Evidence for magmatic injection and recharge at 1·61 Ma as revealed by cathodoluminescence and titanium geothermometry. *Journal of Geology* **117**, 469–485.

Caress, M. E. (1995). Alkali feldspars in the Tshirege Member of the Bandelier Tuff: Systematic vertical and lateral distribution of feldspar compositions and their implications, PhD thesis, University of California, Santa Barbara, 151 pp.

Caress, M. E. (1996). Zonation of alkali feldspar compositions in the Tshirege Member of the Bandelier Tuff in Pueblo Canyon, near Los Alamos, New Mexico.. In: Goff, F., Kues, B. S., Rogers, M. A., McFadden, L. S. & Gardner, J. N. (eds) *New Mexico Geological Society, 47th Field Conference, Guidebook*. Socorro: New Mexico Geological Society. pp. , pp. 275–283.

Cole, J. W., Milner, D. M. & Spinks, K. D. (2005). Calderas and caldera structures: a review. *Earth-Science Reviews* **69**, 1–26.

Downie, N. M. & Heath, R. W. (1970). *Basic Statistical Methods*, 3rd edn. New York: Harper & Row.

Dunbar, N. W. & Hervig, R. W. (1992). Volatile and trace element composition of melt inclusions from the Lower Bandelier Tuff: Implications for magma chamber processes and eruptive style. *Journal of Geophysical Research* **97**, 15151–15170.

Gardner, J. N., Goff, F., Garcia, S. & Hagan, R. C. (1986). Stratigraphic relations and lithologic variations in the Jemez volcanic field, New Mexico. *Journal of Geophysical Research* **91**, 1763–1778.

Gardner, J. N., Sandoval, M. M., Goff, F., Phillips, E. & Dickens, A. (2007). Geology of the Cerro del Medio rhyolite center, Valles

Caldera, New Mexico. In: Kues, B. S., Kelley, S. A. & Lueth, V. W. (eds) *Geology of the Jemez Region II. New Mexico Geological Society 58th Annual Field Conference Guidebook*. Socorro: New Mexico Geological Society. pp. 367–372.

Gardner, J. N., Goff, F., Kelley, S. & Jacobs, E. (2010). Rhyolites and associated deposits of the Valles–Toledo caldera complex. *New Mexico Geology* **32(1)**, 3–18.

Ghiorso, M. S. & Sack, R. O. (1995). Chemical mass transfer in magmatic processes. IV. A revised and internally consistent thermodynamic model for the interpolation and extrapolation of liquid–solid equilibria in magmatic systems at elevated temperatures and pressures. *Contributions to Mineralogy and Petrology* **119**, 197–212.

Gibler, K. (2004). *Postcollapse volcanism in the Valles Caldera, New Mexico: the transition from large volume explosive to small volume effusive eruptions*, MSc thesis, University of Nevada, Las Vegas, 195 pp.

Girard, G. & Stix, J. (2009). Buoyant replenishment in silicic magma reservoirs: Experimental approach and implications for magma dynamics, crystal mush remobilization, and eruption. *Journal of Geophysical Research* **114**, B08203, doi:10.1029/2008JB005791.

Girard, G. & Stix, J. (2010). Rapid extraction of discrete magma batches from a large differentiating magma chamber; the Central Plateau Member rhyolites, Yellowstone Caldera, Wyoming. *Contributions to Mineralogy and Petrology* **160**, 441–465.

Gladney, E. S. & Bower, N. W. (1985). Determination of elemental composition of NBS 278 and NBS 688 via neutron activation and X-ray fluorescence. *Geostandards Newsletter* **9(2)**, 261–262.

Goff, F. (1983). Subsurface structure of Valles Caldera: A resurgent cauldron in northern New Mexico. *Geological Society of America, Abstracts with Programs* **15**, 381.

Goff, F. (2010). The Valles Caldera: New Mexico's supervolcano. *New Mexico Earth Matters* **10(1)**, 1–4.

Goff, F. & Gardner, J. N. (2004). Late Cenozoic geochronology of volcanism and mineralization in the Jemez Mountains and Valles Caldera, north central New Mexico. In: Mack, G. H. & Giles, K. A. (eds) *The Geology of New Mexico—A Geologic History, New Mexico Geological Society Special Volume 11*. Socorro: New Mexico Geological Society, pp. 295–312.

Goff, F. & Gardner, J. N. (2007). Valles Caldera—Second-day road log, Los Alamos to Valle Grande, southern caldera moat, resurgent dome, northern caldera moat, and barbeque at old Baca ranch headquarters. In: Kues, B. S., Kelley, S. A. & Lueth, V. W. (eds) *Geology of the Jemez Region II. New Mexico Geological Society 58th Annual Field Conference Guidebook*. Socorro: New Mexico Geological Society. pp. 53–92.

Goff, F. & Warren, R. G. (2010). Eruption of reverse-zoned upper Tshirege Member, Bandelier Tuff from central vents within Valles Caldera. *Geological Society of America, Annual Meeting (Denver), Abstracts with Programs* **42(5)**, 51.

Goff, F., Warren, R. G., Goff, C. J., Whiteis, J., Kluk, E. & Counce, D. (2007). Comments on the geology, petrography, and chemistry of rocks within the resurgent dome area, Valles Caldera, New Mexico. In: Kues, B. S., Kelley, S. A. & Lueth, V. W. (eds) *Geology of the Jemez Region II. New Mexico Geological Society 58th Annual Field Conference Guidebook*. Socorro: New Mexico Geological Society. pp. 354–362.

Goff, F., Gardner, J. N., Reneau, S. L., Kelley, S. A., Kempter, K. & Lawrence, J. R. (2011). Geologic map of the Valles Caldera, New Mexico, New Mexico Bureau of Geology and Mineral Resources, Map GM-79, 1:50 000 scale map (colour) and 30 page booklet. World Wide Web Address: http://geoinfo.nmt.edu/publications/maps/geologic/gm/home.cfm.

Götze, J., Plötze, M. & Trautmann, T. (2005). Structure and luminescence characteristics of quartz from pegmatites. *American Mineralogist* **90**, 13–21.

Griggs, R. L. (1964). *Geology and groundwater resources of the Los Alamos area, New Mexico, US Geological Survey Water-Supply Paper* **1735**, 107 pp.

Gualda, G. A. R., Ghiorso, M. S., Lemons, R. V. & Carley, T. L. (2012). Rhyolite-MELTS: A modified calibration of MELTS optimized for silica-rich, fluid-bearing magmatic systems. *Journal of Petrology* **53**, 875–890.

Hayden, L. A. & Watson, E. B. (2007). Rutile saturation in hydrous siliceous melts and its bearing on Ti-thermometry of quartz and zircon. *Earth and Planetary Science Letters* **258**, 561–568.

Heiken, G., Goff, F., Stix, J., Tamanyu, S., Shafiqullah, M., Garcia, S. & Hagan, R. (1986). Intracaldera volcanic activity, Toledo caldera and embayment, Jemez Mountains, New Mexico. *Journal of Geophysical Research* **91**, 1799–1815.

Heiken, G., Goff, F., Gardner, J. N. & Baldridge, W. S. (1990). The Valles/Toledo caldera complex, Jemez Volcanic Field, New Mexico. *Annual Review of Earth and Planetary Sciences* **18**, 27–53.

Hervig, R. L. & Dunbar, N. W. (1992). Cause of chemical zoning in the Bishop (California) and Bandelier (New Mexico) magma chambers. *Earth and Planetary Science Letters* **111**, 97–108.

Hildreth, W. S. (1981). Gradients in silicic magma chambers: implications for lithospheric magmatism. *Journal of Geophysical Research* **86(B11)**, 10153–10192.

Hildreth, W. (2004). Volcanological perspectives on Long Valley, Mammoth Mountain, and Mono Craters: several contiguous but discrete systems. *Journal of Volcanology and Geothermal Research* **136**, 169–198.

Hildreth, W. S. & Wilson, C. J. N. (2007). Compositional zoning in the Bishop Tuff. *Journal of Petrology* **48**, 951–999.

Huang, R. & Audétat, A. (2012). The titanium-in-quartz (TitaniQ) thermobarometer: a critical examination and re-calibration. *Geochimica et Cosmochimica Acta* **84**, 75–89.

Jarosewich, E., Nelen, J. A. & Norberg, J. A. (1980). Reference samples for electron microprobe analysis. *Geostandards Newsletter* **4**, 43–47.

Johannes, W. & Holtz, F. (1996). *Petrogenesis and Experimental Petrology of Granitic Rocks*. Berlin: Springer.

Kennedy, B., Jellinek, M. & Stix, J. (2008). Coupled caldera subsidence and stirring inferred from analogue models. *Nature Geoscience* **1**, 385–389.

Lipman, P. W. (1984). The roots of ash flow calderas in western North America: windows into the tops of granitic batholiths. *Journal of Geophysical Research* **89**, 8801–8841.

Lipman, P. W. (2007). Incremental assembly and prolonged consolidation of Cordilleran magma chambers: Evidence from the Southern Rocky Mountain volcanic field. *Geosphere* **3**, 42–70.

Martí, J., Folch, A., Neri, A. & Macedonio, G. (2000). Pressure evolution during explosive caldera-forming eruptions. *Earth and Planetary Science Letters* **175**, 275–287.

Morgan, G. B. & London, D. (2005). Effect of current density on the electron microprobe analysis of alkali aluminosilicate glasses. *American Mineralogist* **90**, 1131–1138.

Müller, A., Lennox, P. & Trzebski, R. (2002). Cathodoluminescence and micro-structural evidence for crystallisation and deformation processes of granites in the Eastern Lachlan Fold Belt (SE Australia). *Contributions to Mineralogy and Petrology* **143**, 510–524.

Nielson, D. & Hulen, J. (1984). Internal geology and evolution of the Redondo dome, Valles Caldera, New Mexico. *Journal of Geophysical Research* **89**, 8695–8711.

Peppard, B. T., Steele, I. M., Davis, A. M., Wallace, P. J. & Anderson, A. T. (2001). Zoned quartz phenocrysts from the rhyolitic Bishop Tuff. *American Mineralogist* **86**, 1034–1052.

Phillips, E. H. (2004). Collapse and resurgence of the Valles Caldera, Jemez Mountains, New Mexico: $^{40}Ar/^{39}Ar$ age constraints on the timing and duration of resurgence and ages of megabreccia blocks. MSc thesis, New Mexico Institute of Mining and Technology, Socorro, 200 pp.

Phillips, E. H., Goff, F. & Kyle, P. R. (2007*a*). The Deer Canyon and Redondo Creek Members of the Valles Rhyolite Formation: Field relationships, mineral chemistry and magnetite–ilmenite temperature of formation for the Redondo Creek Member. In: Kues, B. S., Kelley, S. A. & Lueth, V. W. (eds) *Geology of the Jemez Region II. New Mexico Geological Society 58th Annual Field Conference Guidebook*. Socorro: New Mexico Geological Society. pp. 90–91.

Phillips, E. H., Goff, F., Kyle, P. R., McIntosh, W. C., Dunbar, N. W. & Gardner, J. N. (2007*b*). The $^{40}Ar/^{39}Ar$ age constraints on the duration of resurgence at the Valles Caldera, New Mexico. *Journal of Geophysical Research* **112**, B08201, doi:10.1029/2006JB004511.

Rowe, M. C., Wolff, J. A., Gardner, J. N., Ramos, F. C., Teasdale, R. & Heikoop, C. E. (2007). Development of a continental volcanic field: petrogenesis of pre-caldera intermediate and silicic rocks and origin of the Bandelier magmas, Jemez Mountains (New Mexico, USA). *Journal of Petrology* **48**, 2063–2091.

Self, S. & Lipman, P. W. (1989). Large ignimbrites and caldera-forming eruptions. In: *IAVCEI Working Group on Explosive Volcanism and Its Products, Guidebook, Field Workshop (11WA) in Jemez Mountains, New Mexico and San Juan Mountains, Colorado*, 1–128.

Self, S., Goff, F., Gardner, J. N., Wright, J. V. & Kite, W. M. (1986). Explosive rhyolitic volcanism in the Jemez Mountains: vent locations, caldera development and relation to regional structure. *Journal of Geophysical Research* **91**, 1779–1798.

Shane, P., Smith, V. C. & Nairn, I. (2005). High temperature rhyodacites of the 36 ka Hauparu pyroclastic eruption, Okataina Volcanic Centre, New Zealand: Change in a silicic magmatic system following caldera collapse. *Journal of Volcanology and Geothermal Research* **147**, 357–376.

Shane, P., Smith, V. C. & Nairn, I. (2008). Millennial timescale resolution of rhyolite magma recharge at Tarawera volcano: insights from quartz chemistry and melt inclusions. *Contributions to Mineralogy and Petrology* **156**, 397–411.

Smith, R. L. (1979). Ash-flow magmatism. In: Chapin, C. E. & Elson, W. E. (eds) *Ash-Flow Tuffs. Geological Society of America, Special Papers* **180**, 5–27.

Smith, R. L. & Bailey, R. A. (1966). The Bandelier Tuff: A study of ash-flow eruption cycles from zoned magma chambers. *Bulletin Volcanologique* **29**, 83–103.

Smith, R. L. & Bailey, R. A. (1968). Resurgent cauldrons. In: Coats, R. R., Hay, R. L. & Anderson, C. A. (eds) *Geological Society of America, Memoirs* **116**, 613–662.

Smith, V., Shane, P. & Nairn, I. (2005). Trends in rhyolite geochemistry, mineralogy, and magma storage during the last 50 kyr at Okataina and Taupo volcanic centres, Taupo Volcanic Zone, New Zealand. *Journal of Volcanology and Geothermal Research* **148**, 372–406.

Smith, V., Shane, P. & Nairn, I. (2010). Insights into silicic melt generation using plagioclase, quartz and melt inclusions from the caldera-forming Rotoiti eruption, Taupo volcanic zone, New Zealand. *Contributions to Mineralogy and Petrology* **160**, 951–971.

Snyder, D. (2000). Thermal effects of the intrusion of basaltic magma into a more silicic magma chamber and implications for eruption triggering. *Earth and Planetary Science Letters* **175**, 257–273.

Sommer, M. A. (1977). Volatiles H_2O, CO_2 and CO in silicate melt inclusions in quartz phenocrysts from the rhyolitic Bandelier air-fall and ash-flow tuff, New Mexico. *Journal of Geology* **85**, 423–432.

Spell, T. L. & Kyle, P. R. (1989). Petrogenesis of Valle Grande Member rhyolites, Valles Caldera, New Mexico: implications for evolution of the Jemez Mountains magmatic system. *Journal of Geophysical Research* **94**, 379–396.

Spell, T. L., Kyle, P. R., Thirlwall, M. F. & Campbell, A. R. (1993). Isotopic and geochemical constraints on the origin and evolution of postcollapse rhyolites in the Valles Caldera, New Mexico. *Journal of Geophysical Research* **98**, 723–739.

Spell, T. L., McDougall, I. & Doulgeris, A. P. (1996). Cerro Toledo Rhyolite, Jemez Volcanic Field, New Mexico: $^{40}Ar/^{39}Ar$ geochronology of eruptions between two caldera-forming events. *Geological Society of America Bulletin* **108**, 1549–1566.

Spera, F. J. & Crisp, J. A. (1981). Eruption volume, periodicity, and caldera area: relationships and inferences on development of compositional zonation in silicic magma chambers. *Journal of Volcanology and Geothermal Research* **11**, 169–187.

Steck, L. K., Thurber, C. H., Fehler, M. C., Lutter, W. J., Roberts, P. M., Baldridge, W. S., Stafford, D. G. & Sessions, R. (1998). Crust and upper mantle *P* wave velocity structure beneath Valles Caldera, New Mexico: Results from the Jemez teleseismic tomography experiment. *Journal of Geophysical Research* **103**, 24301–24320.

Stimac, J. A. (1996). Hornblende-dacite pumice in the Tshirege member of the Bandelier Tuff: Implications for magma chamber and eruptive processes. In: Goff, F., Kues, B. S., Rogers, M. A., McFadden, L. D. & Gardner, J. N. (eds) *New Mexico Geological Society Fall Field Conference Guidebook—47, Jemez Mountains Region*. Socorro: New Mexico Geological Society. pp. 269–274.

Stimac, J., Hickmott, D., Abell, R., Larocque, A. C. L., Broxton, D., Gardner, J., Chipera, S., Wolff, J. & Gauerke, E. (1996). Redistribution of Pb and other volatile trace metals during eruption, devitrification, and vapor-phase crystallization of the Bandelier Tuff, New Mexico. *Journal of Volcanology and Geothermal Research* **73**, 245–266.

Stix, J. F. (1989). *Physical and chemical fractionation processes in subaerial and subaqueous pyroclastic rocks*, PhD thesis, University of Toronto, 365 pp.

Stix, J. & Kobayashi, T. (2008). Magma dynamics and collapse mechanisms during four historic caldera-forming events. *Journal of Geophysical Research* **113**, B09205, doi:10.1029/2007JB005073.

Stix, J. & Layne, G. D. (1996). Gas saturation and evolution of volatile and light lithophile elements in the Bandelier magma chamber between two caldera-forming eruptions. *Journal of Geophysical Research* **101**, 181–196.

Stix, J., Goff, F., Gorton, M. P., Heiken, G. & Garcia, S. R. (1988). Restoration of compositional zonation in the Bandelier silicic magma chamber between two caldera forming eruptions: geochemistry and origin of the Cerro Toledo Rhyolite, Jemez Mountains, New Mexico. *Journal of Geophysical Research* **93**, 6129–6147.

Stix, J., Gauthier, G. & Ludden, J. N. (1995). A critical look at quantitative laser-ablation ICP-MS analysis of natural and synthetic glasses. *Canadian Mineralogist* **33**, 435–444.

Thomas, J. B., Watson, E. B., Spear, F. S., Shemella, P. T., Nayak, S. K. & Lanzirotti, A. (2010). TitaniQ under pressure: the effect of pressure and temperature on the solubility of Ti in quartz. *Contributions to Mineralogy and Petrology* **160**, 743–759.

Vance, J. A. (1969). On synneusis. *Contributions to Mineralogy and Petrology* **24**, 7–29.

Vasquez, J. A., Kyriazis, S. F., Reid, M. R., Sehler, R. C. & Ramos, F. C. (2009). Thermochemical evolution of young rhyolites at Yellowstone: Evidence for a cooling but periodically replenished postcaldera magam reservoir. *Journal of Volcanology and Geothermal Research* **188**, 186–196.

Vernon, R. H. (2004). *A Practical Guide to Rock Microstructure*. Cambridge: Cambridge University Press.

Wark, D. A. & Watson, E. B. (2006). TitaniQ: a titanium-in-quartz geothermometer. *Contributions to Mineralogy and Petrology* **152**, 743–754.

Wark, D. A., Hildreth, W., Spear, F. S., Cherniak, D. J. & Watson, E. B. (2007). Pre-eruption recharge of the Bishop magma system. *Geology* **35**, 235–238.

Warren, R. G., McDonald, E.V. & Ryti, R. T. (1997). *Baseline geochemistry of soil and bedrock Tshirege Member of the Bandelier Tuff at MDA-P, Los Alamos National Laboratory, Report LA-13330-MS*, 89 pp.

Warren, R. G., Goff, F., Kluk, E. C. & Budahn, J. R. (2007). Petrography, chemistry, and mineral compositions for subunits of the Tshirege member, Bandelier Tuff within the Valles Caldera and Pajarito Plateau. In: Kues, B. S., Kelley, S. A. & Lueth, V. W. (eds) *Geology of the Jemez Region II. New Mexico Geological Society 58th Annual Field Conference Guidebook*. Socorro: New Mexico Geological Society. pp. 316–332.

Warshaw, C. M. & Smith, R. L. (1988). Pyroxenes and fayalites in the Bandelier Tuff, New Mexico: temperatures and comparison with other rhyolites. *American Mineralogist* **73**, 1025–1037.

Wiebe, R. A., Wark, D. A. & Hawkins, D. P. (2007). Insights from quartz cathodoluminescence zoning into crystallization of the Vinalhaven granite, coastal Maine. *Contributions to Mineralogy and Petrology* **154**, 439–453.

Wolff, J. A. & Gardner, J. N. (1995). Is the Valles Caldera entering a new cycle of activity? *Geology* **23**, 411–414.

Wolff, J. A., Balsley, S. D. & Gregory, R. T. (2002). Oxygen isotope disequilibrium between quartz and sanidine from the Bandelier Tuff, New Mexico, consistent with a short residence time of phenocrysts in rhyolitic magma. *Journal of Volcanology and Geothermal Research* **116**, 119–135.